To the Graduate Council:

I am submitting herewith a thesis written by John Marcus Legan entitled "Mössbauer Studies of ^{237}Np in a Synthetic Monazite." I recommend that it be accepted in partial fulfillment of the requirements for the degree of Master of Science, with a major in Physics.

Paul G. Huray, Major Professor

We have read this thesis and recommend its acceptance:

John O Thomson

Joseph R Peterson

Accepted for the Council:

L Evans Haak
Vice Chancellor
Graduate Studies and Research

MÖSSBAUER STUDIES OF ^{237}Np IN A SYNTHETIC MONAZITE

A Thesis

Presented for the

Master of Science

Degree

The University of Tennessee, Knoxville

John Marcus Legan

March 1981

ABSTRACT

The nuclear gamma resonance (NGR) for ^{237}Np in the compound $NpPO_4$ has been measured at 4.2 K following the α decay of ^{241}Am metal as a source. NGR was also measured in the compound NpO_2 at 4.2 K and 77 K following the α decay of ^{241}Am in the compound $AmPO_4$. In both cases the Np is in a synthetic monazite composed primarily of the compound $LaPO_4$, an insulator. The isomer shift has been determined from the data and indicates a single charge state for Np in $NpPO_4$ and multiple charge states for Np following α decay of Am in $AmPO_4$.

ABSTRACT

The nuclear gamma resonance (NGR) for ^{237}Np in the compound $NpPO_4$ has been measured at 4.2 K following the α decay of ^{241}Am metal as a source. NGR was also measured in the compound NpO_2 at 4.2 K and 77 K following the α decay of ^{241}Am in the compound $AmPO_4$. In both cases the Np is in a synthetic monazite composed primarily of the compound $LaPO_4$, an insulator. The isomer shift has been determined from the data and indicates a single charge state for Np in $NpPO_4$ and multiple charge states for Np following α decay of Am in $AmPO_4$.

TABLE OF CONTENTS

LIST OF TABLES

LIST OF FIGURES

FIGURE PAGE

CHAPTER I

INTRODUCTION

The motivation for this work arises from an interest in the use of crystals as a means of isolating radioactive wastes.[1] ^{237}Np, ^{239}Pu, ^{241}Am and ^{246}Cm are all α-active components of nuclear reactor waste and have half-lives ranging from 500 to 2 million years. The idea of binding radioactive elements in a crystal suggests itself in nature by the presence of monazite, a natural rare-earth phosphate which is known to contain significant amounts of uranium and thorium. The mineral is known to have a physical lifetime of more than a billion years. Monazite is primarily lanthanum orthophosphate ($LaPO_4$). A project at Oak Ridge National Laboratory, under which this work was carried out, has successfully incorporated several α-active transuranic isotopes in synthetic monazite. A number of studies have been carried out on these synthetic crystals including electron spin resonance analysis, X-ray analysis, optical transmission spectroscopy, leaching studies, and Mössbauer studies.[2] All of the studies in this experimental program are aimed at determining the applicability of α-active waste isolation with synthetic monazite, especially those which are more active than the uranium and thorium compounds found in nature. Developmental work on solid state isolation techniques has been earmarked as a top priority in research[3] and shows promise for a dependability which may be greater than any of the other waste forms studied to date.

I. Mössbauer Spectroscopy

Mössbauer spectroscopy has long been recognized as a valuable tool for the study of solid state properties of atoms in crystals. Through hyperfine interactions, information may be obtained about the local magnetic field, the electric field gradient at the lattice site, and most importantly for this work, the oxidation state of the atom.

The Mössbauer effect, or recoilless absorption of nuclear γ-rays, was first observed by R. L. Mössbauer.[4] Over the years since Mössbauer's discovery a number of considerations have been found to affect the suitability of a particular isotope for Mössbauer spectroscopy. One of the most important factors is the energy of the γ-transition which must be low in order to minimize the recoil of the emitting and absorbing atoms. Only when the emitting and absorbing atoms impart all of their recoil to the surrounding crystal lattice as a whole does resonant γ-ray absorption occur. The fraction of γ-ray absorptions can be maximized by reducing the energy of the crystal lattice by cooling. Other factors are a significantly large lifetime of the excited nuclear state which gives rise to the γ-ray and a mechanism for easily populating the excited state (usually through a natural decay process). The full widths at half maximum (FWHM) of the γ-resonance, Γ, follows the relation:[5]

$$\Gamma \cdot \tau \simeq h/2\pi \qquad (1)$$

where τ is the mean-life of the excited state and h is Planck's constant. Thus the shorter the mean-life of the excited state, the broader will

be the γ-resonance. This natural linewidth of the resonance is the limiting factor in probing any of the effects which show up in the hyperfine structure if it is large compared to the electric monopole, magnetic dipole, or electric quadrupole hyperfine interactions.

In this work the α-decay of ^{241}Am to ^{237}Np is used to populate the 59.54 keV excited level of $^{237}Np^{*}$ (Figure 1).[6] The excited nuclear state has a half-life of 68 ns and gives rise to a natural linewidth of $\sim 10^{-8}$ eV. Γ may be related to the Doppler velocity by the equation:[5]

$$v = c\,\Gamma/E_0 \qquad (2)$$

where c is the velocity of light and E_0 is the energy of the γ-resonance. This gives a linewidth of approximately .07 mm/sec for the 59.54 keV transition. No one has ever come close to this value experimentally. The best observed is about 1 mm/sec as reported by Kalvius.[7] Even though it is far from the natural linewidth, it is narrow enough to show very small hyperfine interactions. This fact along with the large percentage (85%) of the ^{241}Am α-decays which go to the 59.54 keV excited level of ^{237}Np has long established this isotope as the workhorse of actinide Mössbauer studies.

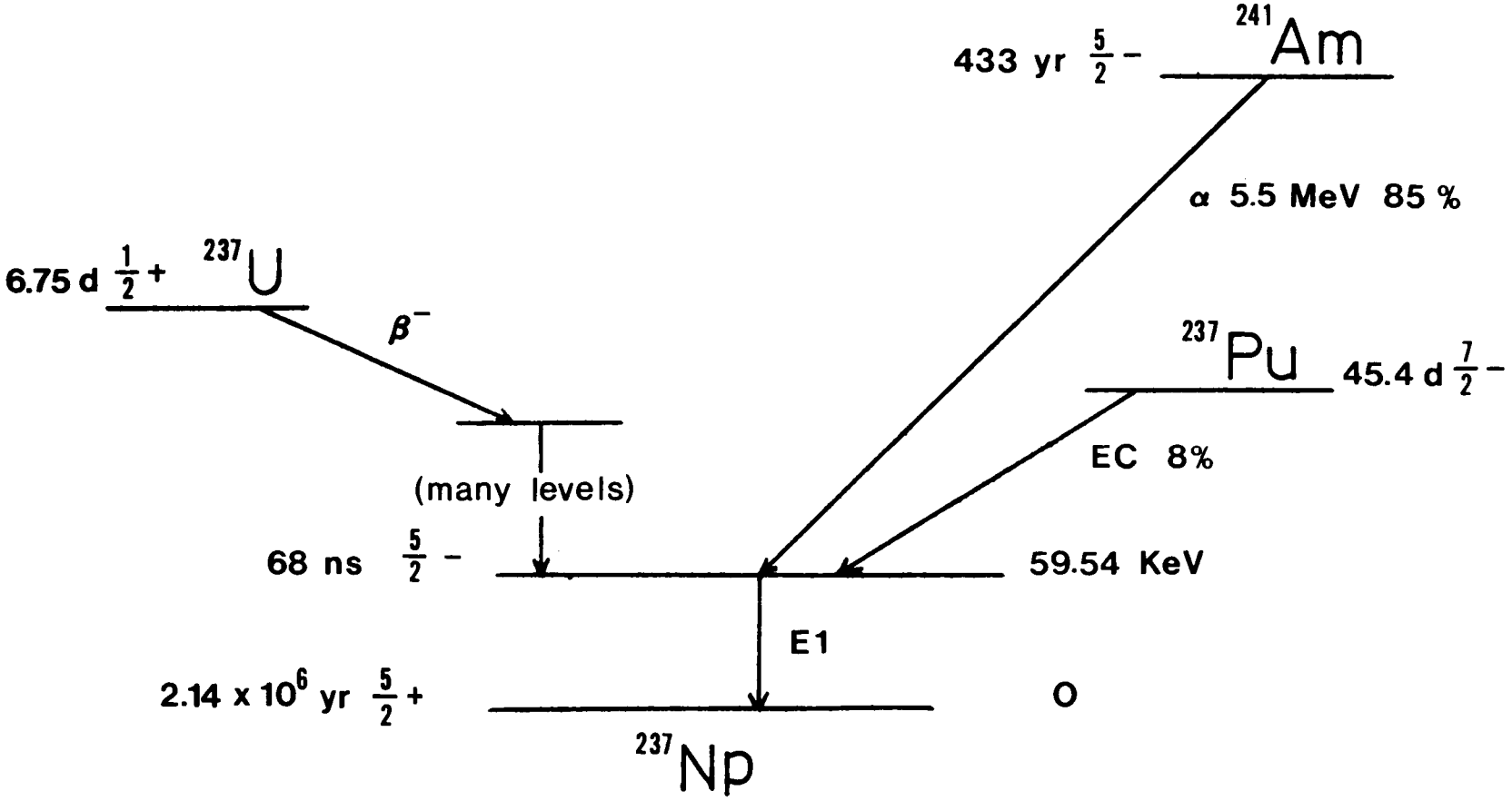

Figure 1. Simplified decay schemes to the 59.54 keV $^{237}Np^{*}$ level.

CHAPTER II

THEORY

As a result of electric and magnetic interactions between the nucleus and its environment, subtle differences may exist between the excited and ground state of the nucleus. These interactions are known as the nuclear hyperfine interactions and in this work three of them are considered as potentially important in the analysis of the data. One can write the interaction Hamiltonian as:

$$\hat{H} = \hat{H}_{IS} + \hat{H}_{Q} + \hat{H}_{M} \ . \tag{3}$$

The first two terms, H_{IS} and H_{Q}, arise from the first two terms in the multipole expansion of the electric interaction between the charge of the nucleus and the surrounding electronic charge. H_{IS} is the monopole, $\ell = 0$, term and H_{Q} is the quadrupole, $\ell = 2$, term. There are no odd terms in the expansion ($\ell = 1, 3, \ldots$) since they vanish when the nuclear wavefunction is an eigenfunction of parity.[8] H_{M} on the other hand interacts with the odd terms.

Figure 2 shows the effect of the terms H_{Q} and H_{M} on the $^{237}Np^{*} \rightarrow {}^{237}Np$ transition.[9] The splitting of the nuclear energy levels (if larger than the FWHM) can partially destroy the resonance effect between the source and the absorber. The nuclear γ-resonance may be restored by Doppler shifting the source relative to the absorber. The Doppler velocity is shown on the horizontal axis and corresponding typical Mössbauer spectra are shown in Figure 2b. The change in energy of the emitted γ-ray as a result of the Doppler shift is given by:[5]

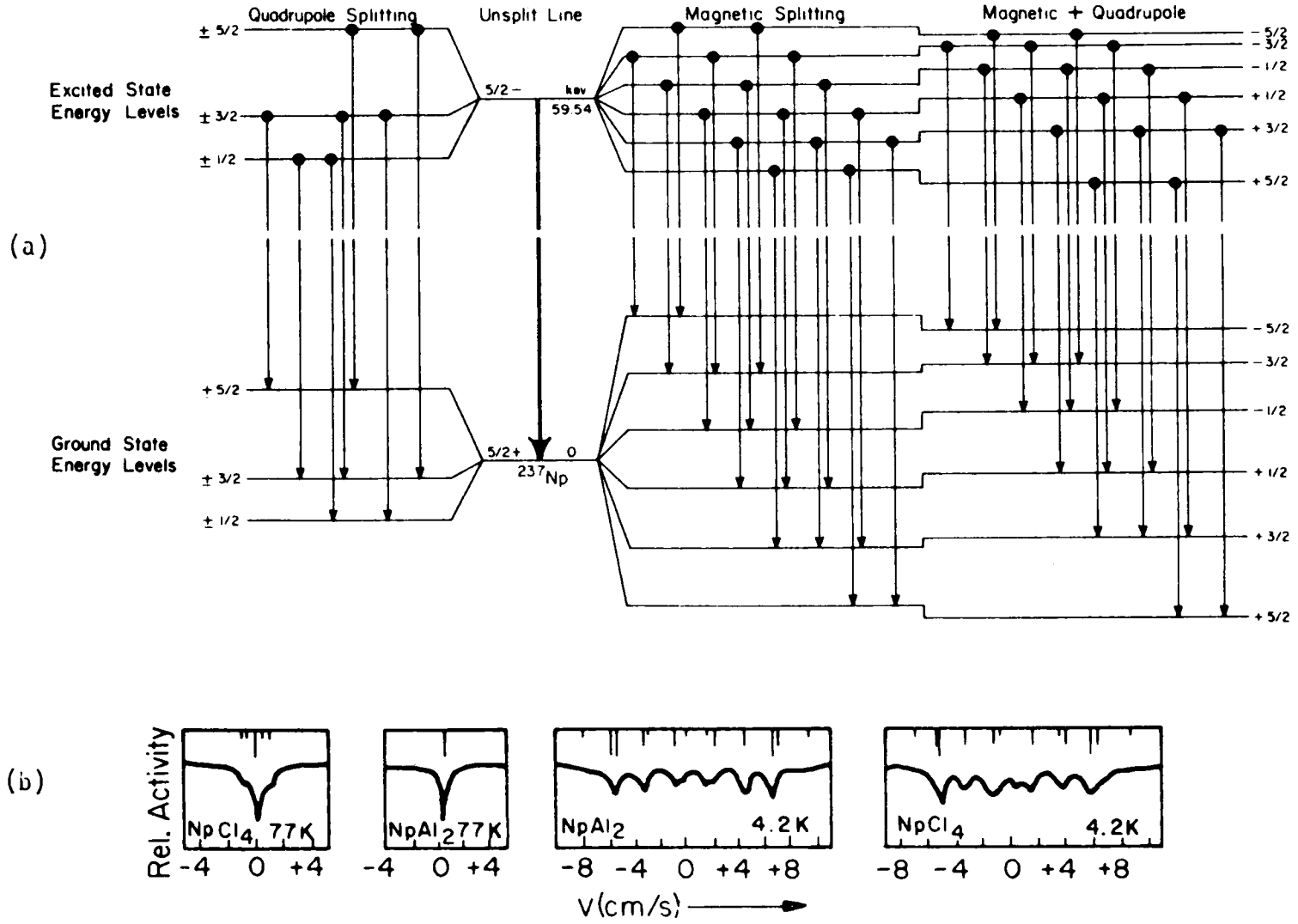

Figure 2. Energy splitting of ^{237}Np 59.54 keV 5/2-, 5/2+ transition due to quadrupole, magnetic and combined interactions. (From Ref. 9.)

$$\Delta E = E_\gamma v/c \tag{4}$$

where E_γ is the energy of the emitted γ-ray, v is the Doppler velocity, and c is the velocity of light.

Of particular interest in this work is H_{IS} which does not introduce any splitting of the energy levels but rather a net shift of the γ-ray energy. This is observed when the $^{237}Np^*$ source and the ^{237}Np absorber are in different chemical environments (thus the synonym "chemical shift") corresponding to different oxidation states. (This is not the only source of an isomer shift, but it is the prominent one in this work.) Again, the resonance condition may be partially destroyed and may be restored according to Equation (4) by Doppler shifting the source relative to the absorber.

I. Electric Hyperfine Interactions

Let us consider first the electrostatic energy of interaction between the nuclear charge and the electronic charge. The expectation value of the Coulomb interaction energy is given by:

$$H_e = -e^2 \int_N \int_E \frac{\rho_N(\vec{r}_N)\,\rho_E(\vec{r}_E)}{|\vec{r}_N - \vec{r}_E|}\, d\tau_E d\tau_N \tag{5}$$

where $\rho_N(\vec{r}_N)$ and $\rho_E(\vec{r}_E)$ are the nuclear and electronic charge distributions (with e and -e factored out, respectively) and $d\tau_E$ and $d\tau_N$ are the volume elements as shown in Figure 3.[10] If the spherical harmonic expansion of $1/|\vec{r}_N - \vec{r}_E|$ is used

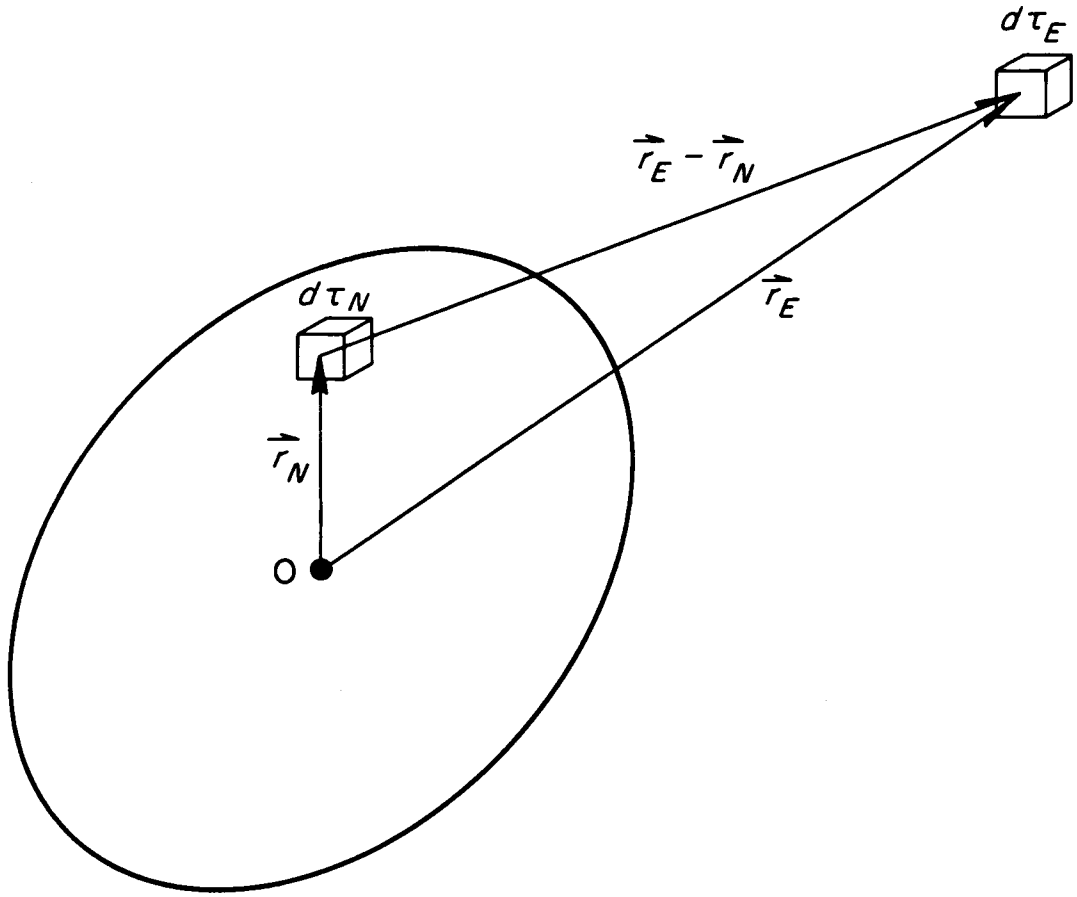

Figure 3. Interaction between nuclear charge density (ρ_N, $\vec{r}_N$) and electronic charge density (ρ_E, $\vec{r}_E$).

$$\frac{1}{|\vec{r}_N - \vec{r}_E|} = 4\pi \sum_{\ell=0}^{\infty} \sum_{m=-\ell}^{\ell} \frac{1}{2\ell + 1} \frac{r_<^{\ell}}{r_>^{\ell+1}} Y_{\ell m}^{*}(\theta_N, \phi_N) Y_{\ell m}(\theta_E, \phi_E) \ . \quad (6)$$

In Equation (6) the $Y_{\ell m}$ are the spherical harmonics and $r_<$, $r_>$ refer to the smaller and larger (respectively) of $|\vec{r}_E|$ and $|\vec{r}_N|$.

II. Isomer Shift

The term in the spherical harmonic expansion corresponding to $\ell = 0$ leads to the monopole term in the interaction energy:[11]

$$H_{IS} = -e^2 \int_N \int_E \frac{\rho_N(\vec{r}_N)\rho_E(\vec{r}_E)}{r} d\tau_E d\tau_N \ . \quad (7)$$

Integrating over angular coordinates, this leads to:

$$H_{IS} = -(4\pi e)^2 \int_{r_N} \int_{r_E} \frac{\rho_N'(r_N)\rho_E'(r_E)}{r_>} r_E^2 dr_E r_N^2 dr_N \quad (8)$$

where $\rho_N'(r_N)$ and $\rho_E'(r_E)$ are the angularly averaged charge distributions, or:

$$\rho'(r) = \frac{1}{4\pi} \int \rho(\vec{r}) \sin\theta d\theta d\phi \ . \quad (9)$$

Breaking this integral over electronic coordinates into spatial regions, one may write:

$$H_{IS} = -(4\pi e^2) \int_0^{\infty} \left[\int_0^{r_N} \frac{\rho_E'(r_E) r_E^2 dr_E}{r_N} + \int_{r_N}^{\infty} \frac{\rho_E'(r_E) r_E^2 dr_E}{r_E} \right] \rho_N'(r_N) r_N^2 dr_N \, . \tag{10}$$

Rewriting the second term as:

$$\int_{r_N}^{\infty} \frac{\rho_E'(r_E) r_E^2 dr_E}{r_E} = \int_0^{\infty} \frac{\rho_E'(r_E) r_E^2 dr_E}{r_E} - \int_0^{r_N} \frac{\rho_E'(r_E) r_E^2 dr_E}{r_E} \tag{11}$$

allows us to rewrite (10) as:

$$H_{IS} = -(4\pi e^2) \int_0^{\infty} \int_0^{r_N} \left(\frac{1}{r_N} - \frac{1}{r_E} \right) \rho_E'(r_E) \rho_N'(r_N) r_E^2 r_N^2 dr_E dr_N$$

$$-(4\pi e)^2 \int_0^{\infty} \frac{\rho_E'(r_E) r_E^2 dr_E}{r_E} \int_0^{\infty} \rho_N'(r_N) r_N^2 dr_N \, . \tag{12}$$

This last expression is in an extremely useful form. Notice that the second term is just the Coulomb interaction energy between a point nucleus and the surrounding electrons. We will designate the second term H_0 where:

$$H_0 = + ZeV \tag{13}$$

where

$$V = -e \int_E \frac{\rho_E(\vec{r}_E)}{|\vec{r}_E|} d\tau_E \tag{14}$$

and

$$Z = \int_N \rho_N(\vec{r}_N) d\tau_N \ . \tag{15}$$

Now, defining δ to be $H_{mon} - H_o$, which is the electrostatic variation due to the finite size of the nucleus exclusive of the point nucleus interaction energy:

$$\delta = -(4\pi e)^2 \int_0^{\infty} \int_0^{r_N} \left(\frac{1}{r_N} - \frac{1}{r_E} \right) \rho_E'(r_E) \rho_N'(r_N) r_E^2 dr_E r_N^2 dr_N \ . \tag{16}$$

Up to this point the solution for δ has been exact. In the usual derivation of this term the assumption is now made that $\rho_E'(r_E) \rightarrow \rho_E'(0) = |\psi(0)|^2$. Monard et al.[12] have investigated the variation of δ when the assumptions of uniform electron density and spherical nuclear charge distribution are not made. By considering two effects: (1) the variation of the relativistic electron wave function interior to a uniformly charged sphere of radius R_o, and (2) the effect of a nonspherical nuclear charge distribution (no attempt was made to compute the variation of the electron wave function due to the non-spherical nuclear charge), they were able to show that a worst possible case gave a variation of δ of 4.5% which corresponds to the case of no nuclear distortion. For parameters observed for ^{234}U, the variation was seen to be less than 2%. It is believed (although calculations were not

carried out in this work) that the variation in δ is also negligible for ^{237}Np and the assumption $\rho_E'(r_E) \rightarrow \rho_E'(0) = |\psi(0)|^2$ will be adhered to in the subsequent derivation.

Rewriting (16) we have:

$$\delta \simeq -(4\pi e)^2 |\psi(0)|^2 \int_0^\infty \rho_N'(r_N) \left[\int_0^{r_N} \left(\frac{r_E^2}{r_N} - r_E \right) dr_E \right] r_N^2 dr_N \, . \qquad (17)$$

Evaluating the integral in brackets we have:

$$\delta \simeq \frac{2}{3} \pi e^2 |\psi(0)|^2 \left(4\pi \int_0^\infty \rho_N'(r_N) r_N^4 dr_N \right) . \qquad (18)$$

Note that:

$$Z \langle r_N^2 \rangle = \int_N r_N^2 \rho_N(\vec{r}_N) d\tau_N \qquad (19)$$

or

$$Z \langle r_N^2 \rangle = 4\pi \int_0^\infty \rho_N'(r_N) r_N^4 dr_N \, . \qquad (20)$$

Rewriting (18):

$$\delta \simeq \frac{2}{3} \pi e^2 |\psi(0)|^2 \, Z \langle r_N^2 \rangle \, . \qquad (21)$$

We may now write an expression for the difference in energy between a γ-ray emitted from a finite nucleus in an excited state and

that expected from a finite nucleus in a ground state through the $\ell = 0$ term with the surrounding electronic charge. The expression is

$$\delta_{ex} - \delta_{gr} = \frac{2}{3}\pi Ze^2|\psi(0)|^2 \left(\langle r_N^2\rangle_{ex} - \langle r_N^2\rangle_{gr}\right) . \tag{22}$$

Finally, the experimentally observable isomer shift arises when the Mössbauer source and absorber have different values of $|\psi(0)|^2$. The full expression is then:

$$\delta_{IS} = \frac{2}{3}\pi Ze^2(\langle r_N^2\rangle_{ex} - \langle r_N^2\rangle_{gr})(|\psi_a(0)|^2 - |\psi_s(0)|^2) . \tag{23}$$

It is apparent in this formula for the isomer shift that two conditions must be satisfied for this term to be nonvanishing. First, there must be a variation in the mean square radius between the excited and the ground state of the nucleus. Second, there must be a difference in the electronic wave function at the nucleus between the Mössbauer source and absorber.

One final refinement needs to be made in Eq. (23) to make it consistent with another common form of this result. It is convenient to describe the nucleus as a uniform distribution out to a radius R. So, we can write:

$$\rho_N'(r_N) = \frac{3Z}{4\pi R^3} \quad , \quad r_N < R . \tag{24}$$

Then according to Eq. (20):

$$\langle r_N^2 \rangle = \frac{4\pi}{Z} \int_0^R r_N^4 \frac{3Z}{4\pi R^3} dr_N \tag{25}$$

or

$$\langle r_N^2 \rangle = \frac{3}{5} R^2 \tag{26}$$

where R is referred to as the "equivalent" nuclear radius. Including this in Eq. (23) we have:

$$\delta_{IS} = \frac{4\pi}{5} Ze^2 \frac{\Delta R}{R} R^2 \left(|\psi_a(0)|^2 - |\psi_s(0)|^2 \right) \tag{27}$$

where $\Delta R = R_{ex} - R_{gr}$ (R_{ex} and R_{gr} are the "equivalent" nuclear radii for the excited and ground states).

III. Electric Quadrupole Interaction

In the consideration of the multipole expansion, odd terms are omitted since the nuclear wave function is an eigenstate of parity. Thus, the next term of interest is the $\ell = 2$ term, the quadrupole term. Terms of higher order are only rarely of concern and will be omitted from the present discussion.

The quantum mechanical operator for the quadrupole interaction has been worked out by Monard[10] and is given by:

$$\hat{H}_Q = \frac{eq\,Q}{4I(2I-1)} \left[(3\hat{I}_z^2 - \hat{I}^2) + \frac{1}{2} n (\hat{I}_+^2 + \hat{I}_-^2) \right] \tag{28}$$

where $\hat{I}$, $\hat{I}_z$, $\hat{I}_+$ and $\hat{I}_-$ are the nuclear angular momentum operators

($\hat{I}_{\pm} = \hat{I}_x \pm i\hat{I}_y$). The nuclear asymmetry parameter, η, is given by

$$\eta = \left(\frac{\partial^2 V}{\partial x^2} - \frac{\partial^2 V}{\partial y^2}\right) \Big/ \left(\frac{\partial^2 V}{\partial z^2}\right) . \tag{29}$$

The x, y and z axes are selected through a principle axis transformation such that:

$$\left|\frac{\partial^2 V}{\partial z^2}\right| \geq \left|\frac{\partial^2 V}{\partial x^2}\right| \geq \left|\frac{\partial^2 V}{\partial y^2}\right| \tag{30}$$

which insures that η takes on values between 0 and 1. Q is the nuclear quadrupole moment, e is the charge of a proton and q is the electric field gradient, $\frac{\partial^2 V}{\partial z^2}$.

Often there will be a high degree of axial symmetry in the crystalline field. When this happens η goes to 0 and the interaction Hamiltonian reduces to a much simpler form:

$$\hat{H}_Q = \frac{eq\,Q}{4I(2I-1)} (3\hat{I}_z^2 - \hat{I}^2) . \tag{31}$$

Figure 2b (p. 6) shows a typical quadrupole spectrum with five lines. These five lines are due to the seven possible transitions through E1 radiation ($\Delta I_z = \pm 1, 0$) shown in the figure. The three transitions corresponding to $\Delta I_z = 0$ are degenerate so that they contribute a single more intense line.[13] The asymmetry parameter, η, alters the relative spacings of the quadrupole splitting in this figure and must therefore be included as a variable in the fitting of the spectrum.

IV. Magnetic Hyperfine Interaction

The final energy term of interest in this work is the magnetic term, H_M. The magnetic dipole moment of the nucleus is given by:[14]

$$\vec{\mu} = \frac{e\hbar}{2M} g \vec{I} \tag{32}$$

where g is the nuclear g-factor, M is the proton mass and $\frac{e\hbar}{2M}$ is called the nuclear magneton, nm, and $\hbar$ is $h/2\pi$. The interaction energy between this moment and the magnetic field at the nucleus is given through the Zeeman interaction and is:

$$H_M = \frac{-\mu}{I} H_{eff} I_z \tag{33}$$

where I_z is the magnetic quantum number and H_{eff} is the effective magnetic field defining the quantization axis. Thus, in a nucleus of angular momentum I there will be 2I + 1 equally spaced levels.

V. Combined Magnetic and Quadrupole Effects

The magnetic interaction generally occurs at low temperatures when magnetic ordering has set in, either ferromagnetic or antiferromagnetic. Magnetic splitting does not preclude the possibility of quadrupole splitting and indeed they often occur simultaneously. Usually $H_M >> H_Q$ so that quadrupole splitting only modifies the more apparent magnetically split spectrum. Examples of these complex spectra abound in the literature.[9] The treatment of the combined case is easily analyzed for the special case when there is an axially symmetric electric

field gradient with V_{zz} aligned parallel or at an angle θ with respect to H_{eff} and with $\frac{1}{4}$ eq Q << gμ H_{eff}. In the general case of nonaxial electric field gradient with V_{zz} at an angle θ to the magnetic field H_{eff}, one must solve a multiparametered Hamiltonian for each nuclear state. Hyperfine patterns can be deduced from the transition energies which can be calculated from the eigenvalues and eigenvectors. This pattern must then be fit to the experimental spectrum to determine isomer shift, gμ H_{eff}, $\frac{1}{4}$ eq Q, η, and θ. "Forbidden" transitions are allowed and the resulting spectrum has 36 lines.[13]

VI. Time Dependent Effects and Multiple Charge States

All of the terms discussed up to now have been time independent. In these effects, the electronic relaxation time is either much faster (as in the case of single line or pure quadrupole splitting) or much slower (as in the case of magnetic splitting) than the lifetime of the emitting nucleus. Mössbauer effect spectra affected by intermediate relaxation effects (i.e., when relaxation is on the order of the lifetime of $^{237}Np^{*}$) have little definition and usually appear as a broad absorption over a range of several cm/sec.[9] However, in some ^{241}Am sources which are good insulators, multiline Mössbauer spectra are observed with the velocities of these lines corresponding closely to the isomer shifts of the different neptunium isomer shifts.[15] Thus, the observed spectra are a distribution at an average time of 98 ns after the initial α-decay event. These distributions were found to depend on (1) original americium oxidation state, (2) the valence of the host lattice, and (3) the temperature of the source.

VII. Self-Consistent Field Calculations

In the application of Formula (27) for the isomer shift it is necessary to have accurate values of the terms $|\psi(0)|_a^2$ and $|\psi(0)|_s^2$ in order to derive reliably the term $\Delta R/R$. Computer codes in operation at Oak Ridge National Laboratory (ORNL) and elsewhere provide calculations of relativistic wave functions for atoms and ions. Table 1 presents the results of these calculations for $|\psi(0)|^2$ for two such codes. The codes in use at ORNL are also capable of computing binding energies, screening constants and charge distributions. Figure 4 shows how $\Delta|\psi(0)|^2$ changes with ionization state for the ^{237}Np ion (free atom).

TABLE I

RELATIVISTIC VALUES OF THE ELECTRON PROBABILITY DENSITY AT THE NUCLEUS FOR ^{237}Np

Oxidation State	Configuration (in Addition to Radon Core)	$\|\psi(0)\|^2$ Hartree-Fock-Slater[a] (10^7 au[c])	$\|\psi(0)\|^2$ Dirac-Fock[b] (10^7 au[c])
(0)	$7s^2\ 6d^1\ 5f^4$	8.57385	8.37390
(I)	$7s^2\ 6d^0\ 5f^4$	8.57400	8.37406
(II)	$7s^1\ 6d^0\ 5f^4$	8.57377	--
(III)	$7s^0\ 6d^0\ 5f^4$	8.57348	8.37360
(IV)	$7s^0\ 6d^0\ 5f^3$	8.57372	8.37381
(V)	$7s^0\ 6d^0\ 5f^2$	8.57399	8.37407
(VI)	$7s^0\ 6d^0\ 5f^1$	8.57430	8.37436
(VII)	$7s^0\ 6d^0\ 5f^0$	8.57463	8.37468

[a]T. C. Tucker, L. D. Roberts, C. W. Nestor, T. A. Carlson, F. B. Malik, Phys. Rev. 178, 998 (1969).

[b]I. M. Band, V. I. Fomichev, Atomic Data and Nuclear Data Tables 23, 295 (1979).

[c]One au is equal to 0.538×10^{24} cm^{-3}.

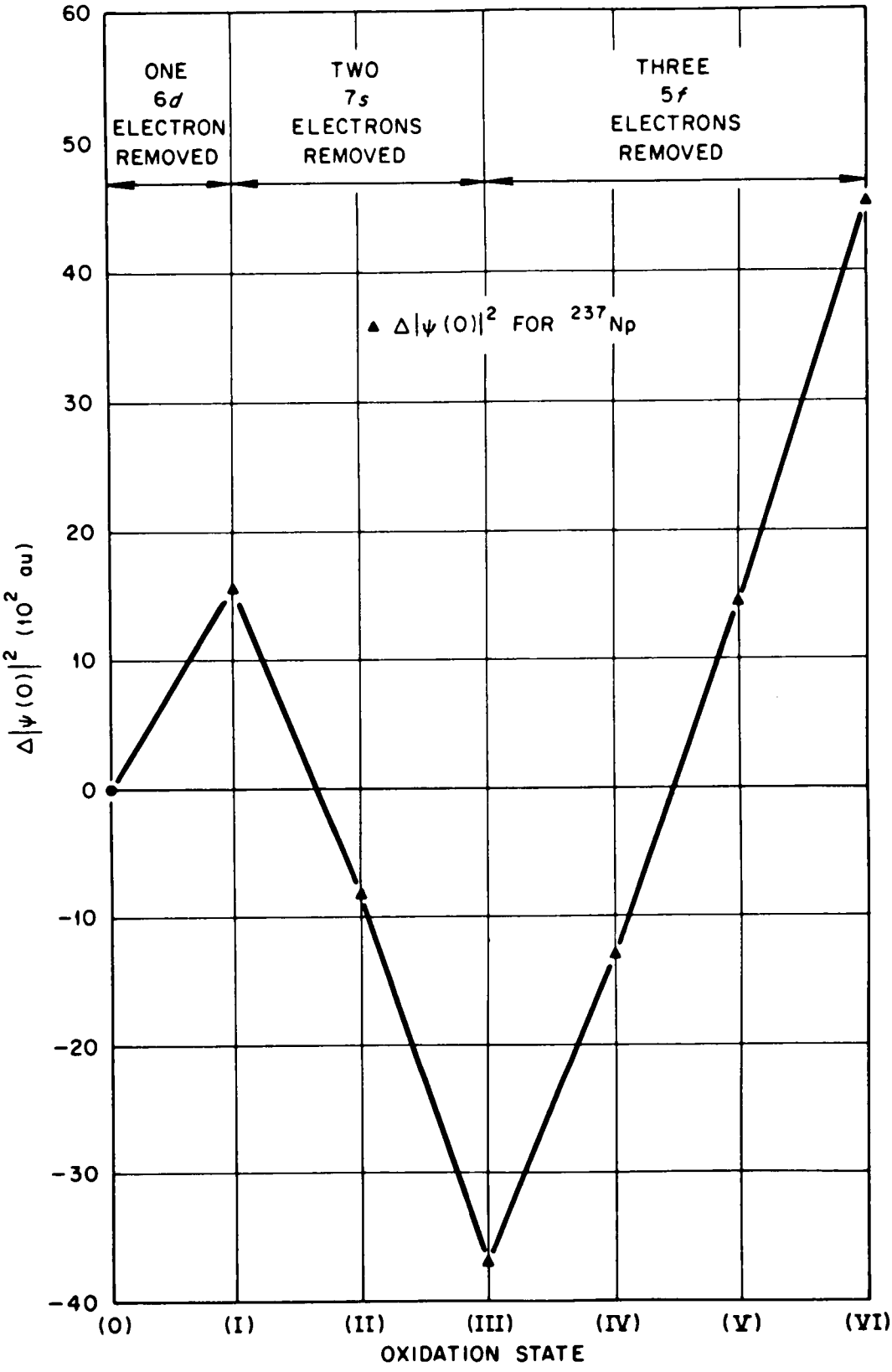

Figure 4. Changes in the relativistic Np electron probability density at the origin with chemical oxidation state for ^{237}Np. One au is equal to 0.538×10^{24} cm^{-3} = $1/(4\pi a_0^3)$.

CHAPTER III

EXPERIMENTAL

I. Health and Safety Precautions

The experiments reported in this thesis were carried out at the Transuranium Research Laboratory (TRL) of Oak Ridge National Laboratory (ORNL). In actinide research extreme care must be taken due to the high radioactivity and chemical toxicity of the elements. ^{237}Np and ^{241}Am are not as radioactive as some of the heavier actinides but among the intermediate lived actinides ^{241}Am is one of the most dangerous. Maximum permissible body burdens for ^{237}Np and ^{241}Am have been set at 709 μg and 8.75×10^{-2} μg respectively.[16] The value for ^{241}Am is only slightly higher than that for ^{238}Pu which is the most toxic nuclear reactor by-product.

The TRL is a laboratory which is unique in that it allows the handling of highly active radioisotopes in a virtually "cold" laboratory environment. The term cold means that the laboratory is virtually contamination free and thus is not considered a contamination zone. This has the advantage of allowing the researcher to move freely about the laboratory unencumbered by elaborate protective clothing or shoe covers. When dealing with samples with an activity of less than 10^6 disintegrations/minute (d/m) the operation may be carried out in a hood. For more active samples a glove box is used. To maintain the cold laboratory environment several containment features are employed. The building ventilation system maintains a .35 inch H_2O negative pressure

with respect to the outside pressure at all times. This is accomplished in three stages. The first is a negative pressure entryway. The corridors are then at a negative pressure with respect to the entryway and finally the labs themselves are at a negative pressure with respect to the corridors. All radioactive samples must remain in the labs which are connected by a central corridor. There is a constant exchange of air in the labs with each laboratory experiencing a turnover of one lab volume of air each three minutes. The air which passes through the lab is filtered by two filter banks. The first bank is an 80% efficiency bank and the second bank has an efficiency of 99.95% for particles of .3 micron diameter. All the air which passes through the filters is continuously monitored for α, β, and γ radiation. Another feature of building safety is a daily testing of all work areas for contamination by Health Physics personnel.

The Mössbauer experiments used the sources shown in Figure 5. Source and absorber materials were sealed in containers and carefully checked for any activity on the surface. Smears taken on the surfaces of the sealed containers in all cases showed less than 5 d/m of activity. This allowed safe handling of the sources and absorbers away from the hood and glove box and so it was easy to load manually the samples on the drive system and into the cryostat. The Am metal source required special handling due to the activity of the sample. Sixty-nine mg of ^{241}Am gives rise to an activity of 236 mCi (1 curie = 3.7×10^{10} d/s) and a 900 mrem/hr γ-ray dose at 2 inches. Sources and absorbers were generally left in the dewar between runs as a means of secondary containment. The dewar had a lead shield affixed to it to reduce the

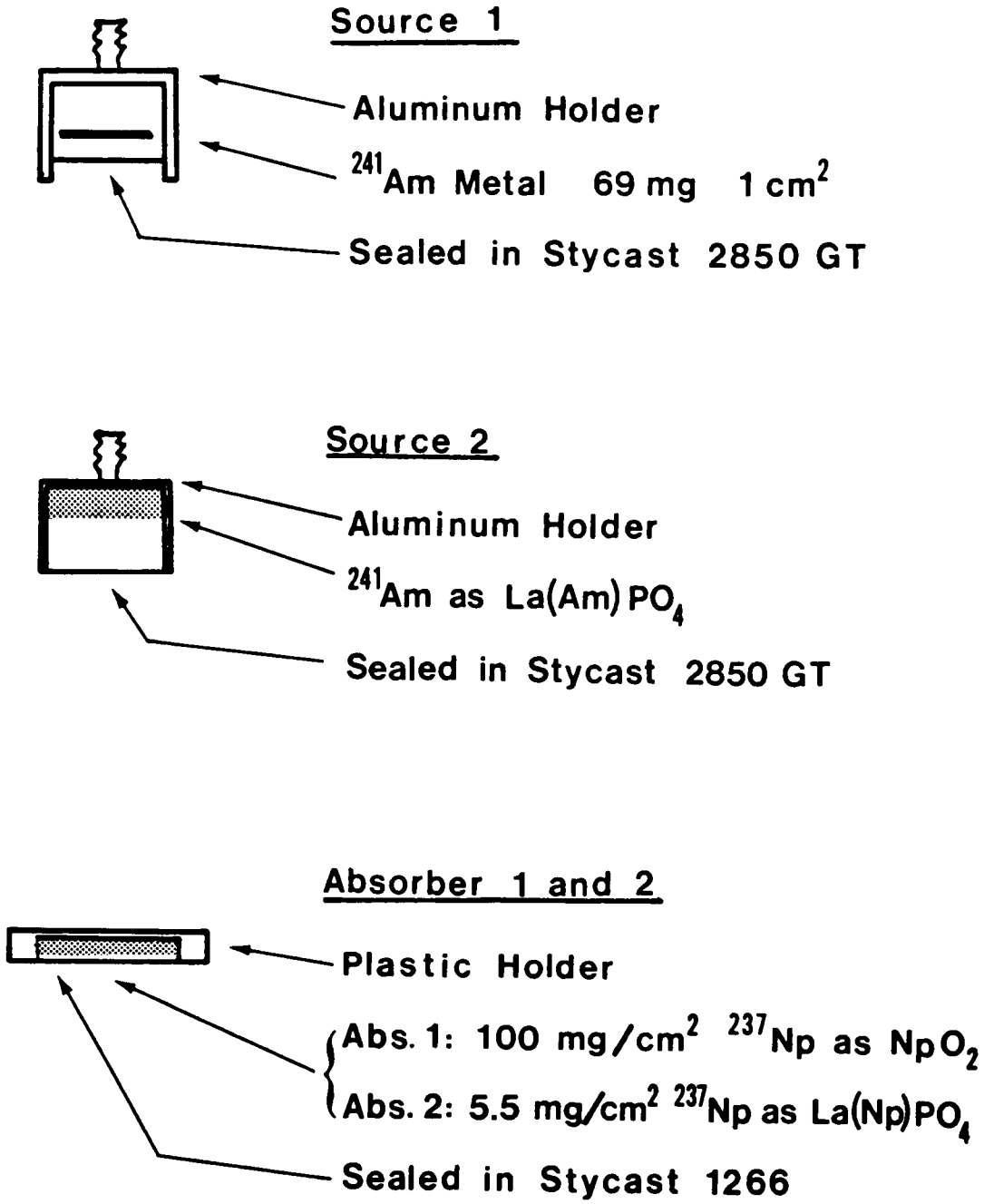

Figure 5. ^{241}Am sources and ^{237}Np absorbers used in the experiment.

γ-ray field in the vicinity of the apparatus. The area around the dewar system was monitored frequently during experiments for α-contamination. The systematic precautions outlined above proved adequate over the duration of the experiment.

II. Source and Absorber Preparation

The preparation of sources and absorbers used in this experiment was carried out by several individuals at ORNL. Although this work will not present an exhaustive description of the techniques employed, references will be cited which give additional information.

The $^{241}AmPO_4$ source and $^{237}NpPO_4$ abosrber were prepared by C. W. Finch using the flux technique described by Fiegelson.[17] The samples prepared in this way have been used for X-ray, leaching, electron paramagnetic, and optical absorption studies as well as Mössbauer spectroscopy. Orthophosphates from the lanthanide series fall into two types. From La to Gd they are characterized by the monoclinic (monazite) structure and from Dy to Lu they have the tetragonal (zircon) structure. The ^{241}Am doped $LaPO_4$ crystals were prepared by starting with .8 weight % in equal amounts of $^{241}Am_2O_3$ and $^{241}AmO_2$ to La_2O_3 and the ^{237}Np doped $LaPO_4$ started as 9 weight % $^{237}NpO_2$ to La_2O_3.[18] Due to an oversight the exact amount of $^{241}AmPO_4$ placed in the source container was not ascertained. An attempt to estimate the amount of ^{241}Am by using a γ-counting technique was hampered by absorption in the La. A rough estimate of the amount of material in the $La(Am)PO_4$ source is 500 mg. In both cases the crystalline material which consisted of rather large crystals was pulverized to a powder using a mortar and pestle in a glove box. This was

done to minimize absorption due to the La with a K X-ray edge (39 keV) which is somewhat below the 59.5 keV γ-ray producing a large cross section for absorption.

It should be noted that the crystal growth process employed for the $^{237}NpPO_4$ absorber and the $^{241}AmPO_4$ source in $LaPO_4$ crystals is not the technique practical for industrial use. The industrial process proposed is similar to the one used by Aaron et al.[19] In this process a precipitation occurs in molten urea. Experiments with $CePO_4$ powders have shown that when the precipitate is hot pressed a density of 98% of the theoretical crystalline density can be formed.[2]

The $^{237}NpO_2$ was obtained from Dick Hahn at TRL. The NpO_2 was heated at 900°C for about 90 minutes while under a reducing atmosphere of 4% hydrogen, 96% argon. This technique suggested by Dick Haire of TRL is designed to guarantee that the nominal NpO_2 is in fact fairly pure. NpO_2 is the most stable oxidation state in which Np exists with oxygen, so passing the hydrogen over the material at high temperature was an effective means of driving off excess oxygen. X-ray analysis of the NpO_2 following the heat treating was performed by Dick Haire and showed a lattice parameter of 5.434(1) Å. The literature value for NpO_2 is 5.425 Å. Thus we are fairly confident of the oxidation state of the Np used in the NpO_2 absorber. Three hundred sixty mg of NpO_2 was used over a surface area of 3.14 cm^2 which gives a density of 100 mg/cm^2 of ^{237}Np.

The ^{241}Am metal source was prepared by Charlie Culpepper of Isotopes Division at ORNL. The ^{241}Am source is a metallic foil 1 cm by 1 cm square and was claimed to have the highest chemical purity of any ever produced at ORNL. It is this source which is depicted in Figure 6

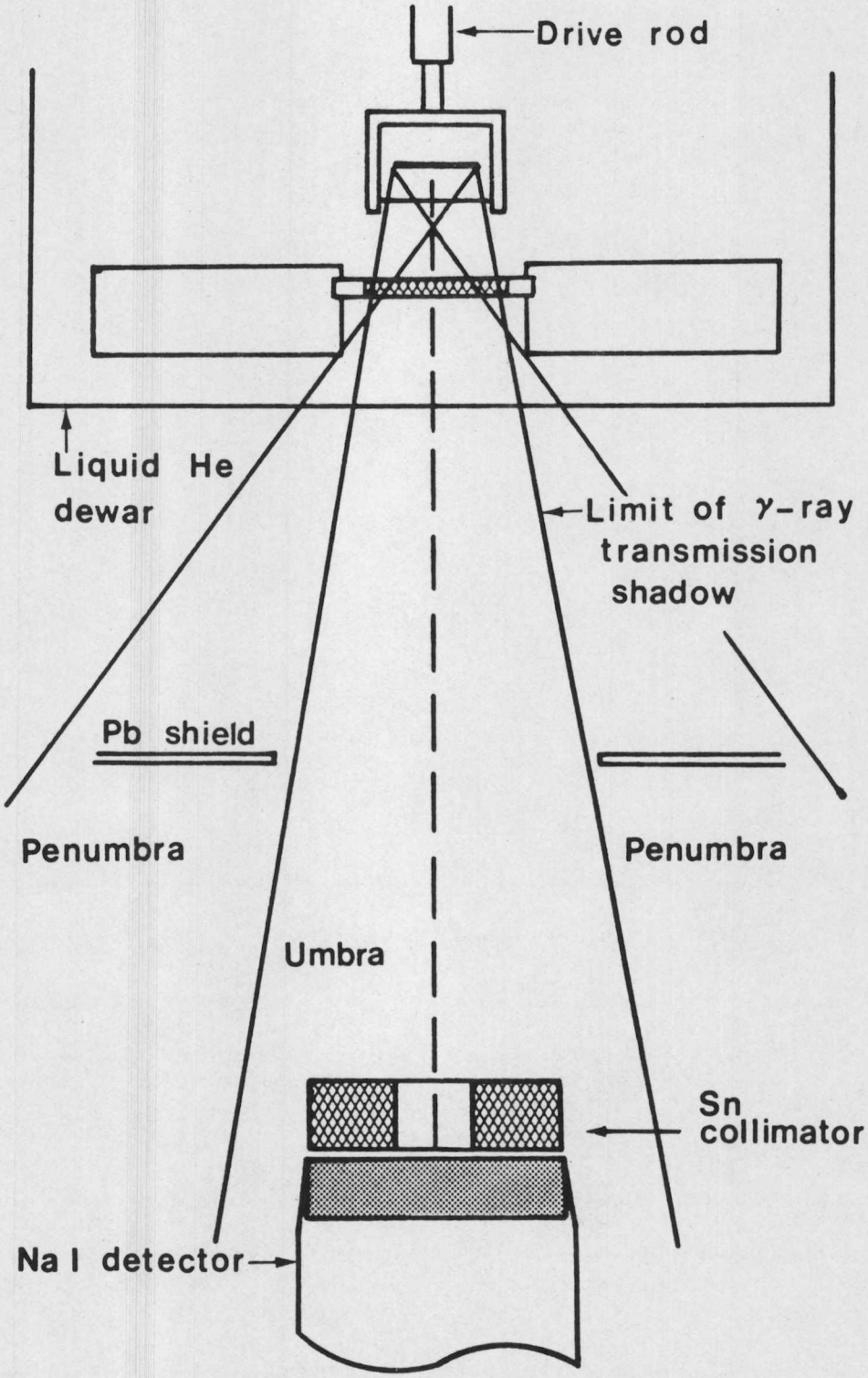

Figure 6. Experimental configuration at the bottom of the dewar system. (Drawn to actual scale.)

showing the maximum extent of the source of 1.414 cm viewed along the diagonal and the γ-ray penumbral and umbral regions produced when transmitted through the apparatus. Table II is a compilation of the source and absorber characteristics for those used in the experiment.

III. Mössbauer Spectrometer

In Np Mössbauer research it is helpful to cool both source and absorber to liquid nitrogen temperature (77 K) or lower in order to get a larger recoilless fraction. With the exception of the Am metal source vs. the NpO_2 absorber statistically poor spectra were observed even at liquid nitrogen temperature and so we chose to cool both source and absorber to liquid helium temperature (4.2 K). Even at 4.2 K the percent effects were small and experiments had to be run from one to three days in order to obtain a satisfactory effect. Low temperatures and extended running times require a liquid helium cryostat with low loss rate and a very stable drive system.

The cryostat used was glass with a central liquid helium cavity surrounded by a liquid nitrogen jacket. A vacuum was maintained between the inner and the outer dewar and between the outer dewar and the outside atmosphere. The liquid helium dewar has a capacity of about 9 liters and with loss rates of about a third of a liter per hour we were able to make runs over a period of several days stopping only once per day to refill with liquid helium. The Am source was connected to a drive assembly by a 77 cm long hollow stainless steel rod and both source and absorber were immersed in liquid helium. The drive system was outside of the dewar at room temperature. In all experiments the source was moved relative to a stationary absorber.

TABLE II

PHYSICAL PROPERTIES OF ^{241}Am SOURCES AND ^{237}Np ABSORBERS

Sample	Weight of Sample (g)	Weight of Radioactive Species in Sample (mg)	^{237}Np Thickness in Absorber (mg/cm^2)	Area of Sample (cm^2)	Activity of Sample (mCi)[a]
Absorber 1: NpO_2	.36	314	100	3.14	.221
Absorber 2:[b] $La(Np)PO_4$	1.15	17.3	5.5	3.14	.012
Source 1: Am metal	.069	69	--	1.0	236
Source 2:[b,c] $La(Am)PO_4$	$\sim$ .5	.95	--	$\sim$ 1.0	$\sim$ 3.3

[a] A mCi (milliCurie) is 3.7×10^7 disintegrations/sec.

[b] Relative amounts of ^{237}Np and ^{241}Am in these samples were determined by dissolving crystals in Na_2CO_3 and leaching into H_2O. The residue was counted for α-activity with the result that 1.9 mg/gm of ^{241}Am present in the $LaPO_4$ source and 15 mg/gm of ^{237}Np present in the $LaPO_4$ absorber. These results were obtained by Carlos Bamberger of ORNL.

[c] The exact amount of $La(Am)PO_4$ placed in the source container was not determined; this is an estimate.

Figure 6 shows the experimental configuration near the bottom of the dewar system. The diagram is greatly simplified to show the important geometrical factors. Not shown in the figure is the nitrogen jacket which extends down around the helium dewar on all sides but does not intervene between the source and the detector. This minimizes the γ-ray absorption by the cryostat. The diagram emphasizes the small tolerances allowable in alignment of the source and absorber since they are so close together. This led to problems in the experiment since the spectra obtained must be corrected for the $1/r^2$ background effect which results from the variation of the separation between the moving source and the detector over the cycle of the source's motion. It became necessary to place a 1 cm diameter tin collimator (tin has a K X-ray edge below 59.5 keV) directly on top of the detector to minimize any partial shadowing effect on the detector crystal.

The 59.5 keV γ-resonance in Np was detected by a 1.25 inch diameter by .5 inch thick Harshaw Integral Line NaI(Tl) detector. The detector was operated at +700 volts. After passing through an Ortec Model 113 preamplifier the pulses from the detector were amplified by a Tennelec TC203 BLR amplifier and baseline restorer. The amplified signal was then passed through a Tennelec TC440 single channel analyzer to select the 59.5 keV γ-resonance. On longer runs it was sometimes necessary to replace the Tennelec TC440 SCA with a Harshaw NA-22 AGC amplifier. This amplifier has an automatic gain control to stay locked on the selected γ-ray. In this way the system was made insensitive to any changes in the detector due to high voltage drift or amplifier instability at the high count rates (often 140,000 counts/sec) encountered.

The block diagram of Figure 7 shows the electronic configuration of the system. In addition to the detector for the Np γ-rays at the bottom of the cryostat it was sometimes necessary to run an ^{57}Fe Mössbauer experiment simultaneously at the top to calibrate the velocity of the drive system. Calibration is made possible by the presence of a high velocity pickup coil housed in the transducer assembly. This pickup coil gives an ac voltage which is an accurate measure of the drive rod velocity. Thus, after initially calibrating the pickup coil using the well-known ^{57}Fe Mössbauer effect it was possible to "dial up" the velocity setting using a Mössbauer drive unit developed by J. O. Thomson.[20] Subsequent determination of the velocity was done by monitoring the rms ac voltage from the pickup coil. The Mössbauer drive unit drives the source rod with the help of a power amplifier. The cosinusoidal driving signal is provided externally by a Krohn-Hite Model 4025R oscillator operating nominally at 20.2 Hz which is close to the natural resonant frequency of the drive rod assembly. The motion of the drive rod is forced to follow the cosinusoidal reference by a feedback loop in the Mössbauer drive unit.

The Krohn-Hite oscillator was synchronized with a Nuclear Data multichannel analyzer (MCA) operated in multiscaling mode. The MCA was stepped by a crystal oscillator also designed by J. O. Thomson. The Krohn-Hite oscillator operated in external synch mode self-adjusted its frequency by a small amount so that the drive unit drove the source rod through one cycle as a single pass was made through the selected set of channels in the MCA. Thus, a given channel in the MCA accumulated γ-rays corresponding to a particular velocity of the source relative to

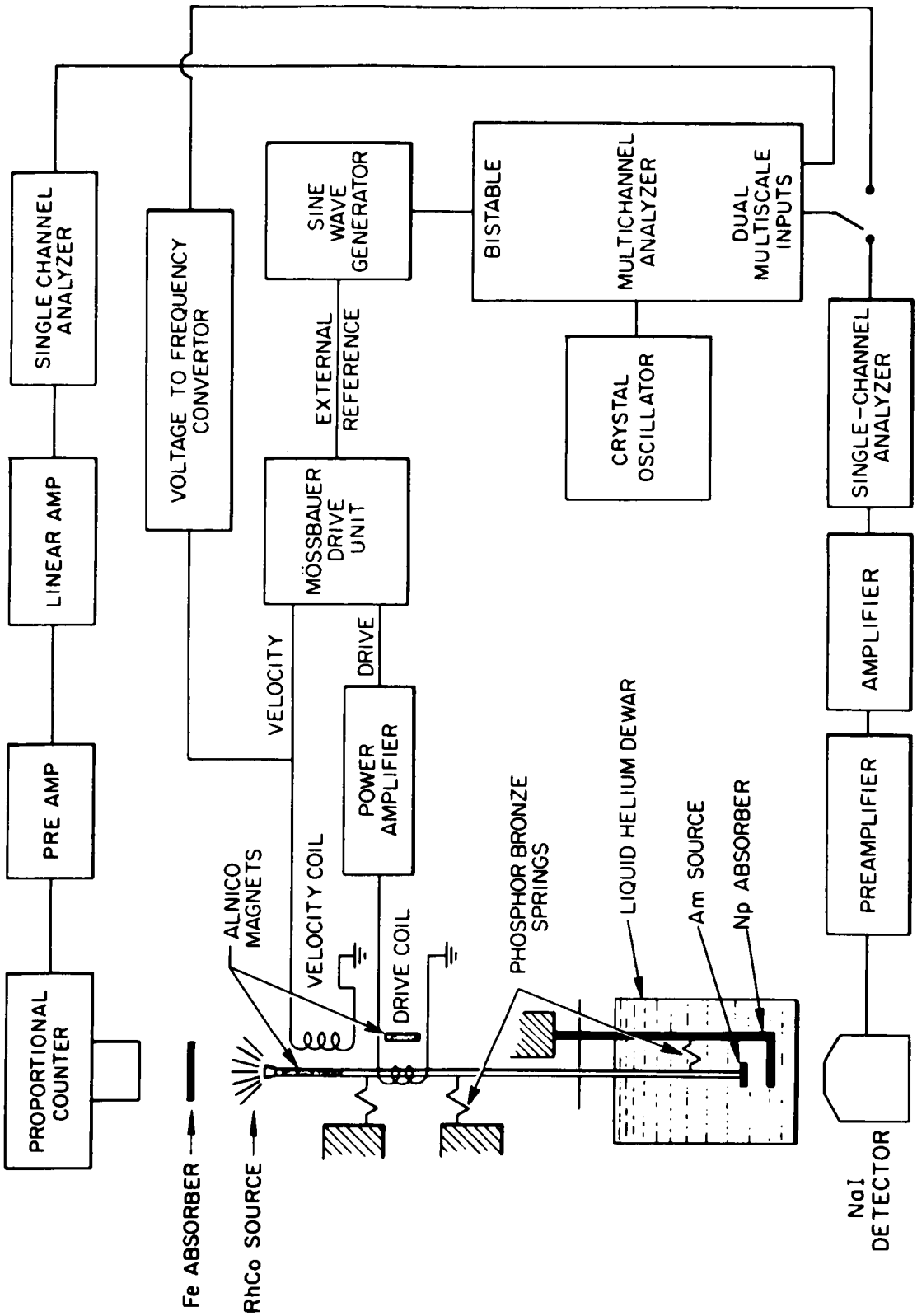

Figure 7. Block diagram of the electronic configuration.

the absorber. Very high resolution was obtained by operating with the MCA stepping over 1024 channels but, usually 256 channels provided adequate resolution.

All of the basic requirements of a Mössbauer spectrometer are provided by the system described above. The system provides a relative velocity between the source and absorber in a controlled and reproducible way and the resonance γ-rays are detected and stored in such a way that they are correlated with instantaneous velocities.

IV. Data Analysis

In addition to the basic spectrometer described above our system was greatly enhanced by the use of a Tektronix 4051 minicomputer. With the minicomputer it was possible to take data from the MCA, store it on magnetic tape, correct it for background distortions caused by the $1/r^2$ effect, associate a proper velocity with each channel, and order the velocities into a single incremental sequence between $-V_{max}$ and $+V_{max}$. The graphics capability of the 4051 then allowed us to display the corrected data on a crt screen or plot it on an x,y plotter. Processed data stored on minicomputer tapes could then be transferred to the DEC10 at ORNL or UT for analysis. The minicomputer was also used to compute the observed line positions in the ^{57}Fe spectrum when calibrating the spectrometer. The Tektronix has a versatile graphics capability which allowed us to visually inspect data manipulations.

The data analysis was usually done in two steps. The first step was to prepare the data on the Tektronix. This involved the removal of the background effect, folding the spectra about the appropriate point

and finally ordering the data by the corresponding velocities. Step by step inspection with the Tektronix graphics display was a great help in assuring the proper corrections on the data.

After the data had been prepared on the Tektronix it was transferred to the DEC10 at UT for fitting. The computer code used fits the spectra by a least squares procedure to a curve of the form:

$$I(V) = B\left[1 - \sum_{i=1}^{N} \frac{A_i}{(V-V_i)^2 + \frac{W_i^2}{4}}\right] \tag{34}$$

where I(V) is the relative intensity at the velocity V, B is a background normalization factor, A_i, V_i, and W_i are the intensity, position, and full width at half maximum for the i^{th} absorption line, and N is the number of absorption lines. It is possible to make any of the parameters A, V, or W variable, constant, or dependent upon some of the other variables. The decision as to which parameters were variable and which were held fixed depended upon the particular spectrum and what information was desired. The least squares routine is said to have converged to the best theoretical fit to the data when the variance is less than some assigned value. The program then solves for an error to associate with each variable indicating the precision to which that value has been calculated.

CHAPTER IV

EXPERIMENTAL RESULTS AND CONCLUSIONS

I. Physical Properties of Sources and Absorbers

The Am metal source and the NpO_2 absorber used in this experiment have been studied extensively in a wide range of experiments. Neptunium is known to be in the oxidation state (IV) in the compound NpO_2. Figure 8 shows a number of other well-characterized compounds of neptunium ranging from the (III) to the (VI) oxidation state. The figure shows the regular arrangement of these compounds by oxidation state when considering quadrupole splitting and oxidation state. The isomer shifts shown are all relative to an NpO_2 absorber and positive velocity implies that the source compound moves toward the absorber (that is, the source γ-rays need a slight increase in Doppler energy for resonant absorption by the NpO_2). Some sources and absorbers defy characterization and cannot be said to belong to a particular oxidation state. One of these is the metallic absorber $NpAl_2$ which lies in the range between (III) and (IV) with an isomer shift of about -6.3 mm/sec relative to NpO_2.[21] Metallic sources and absorbers often fall outside of any known charge state region and this is the case for our Am metal source. With an isomer shift at 7.89 ± .06 relative to the NpO_2 absorber it exhibits a behavior which appears to be more ionized than the (IV) charge state but less than the (V).

In addition to the Mössbauer studies presented in this thesis a number of other studies were done at ORNL to characterize the synthetic

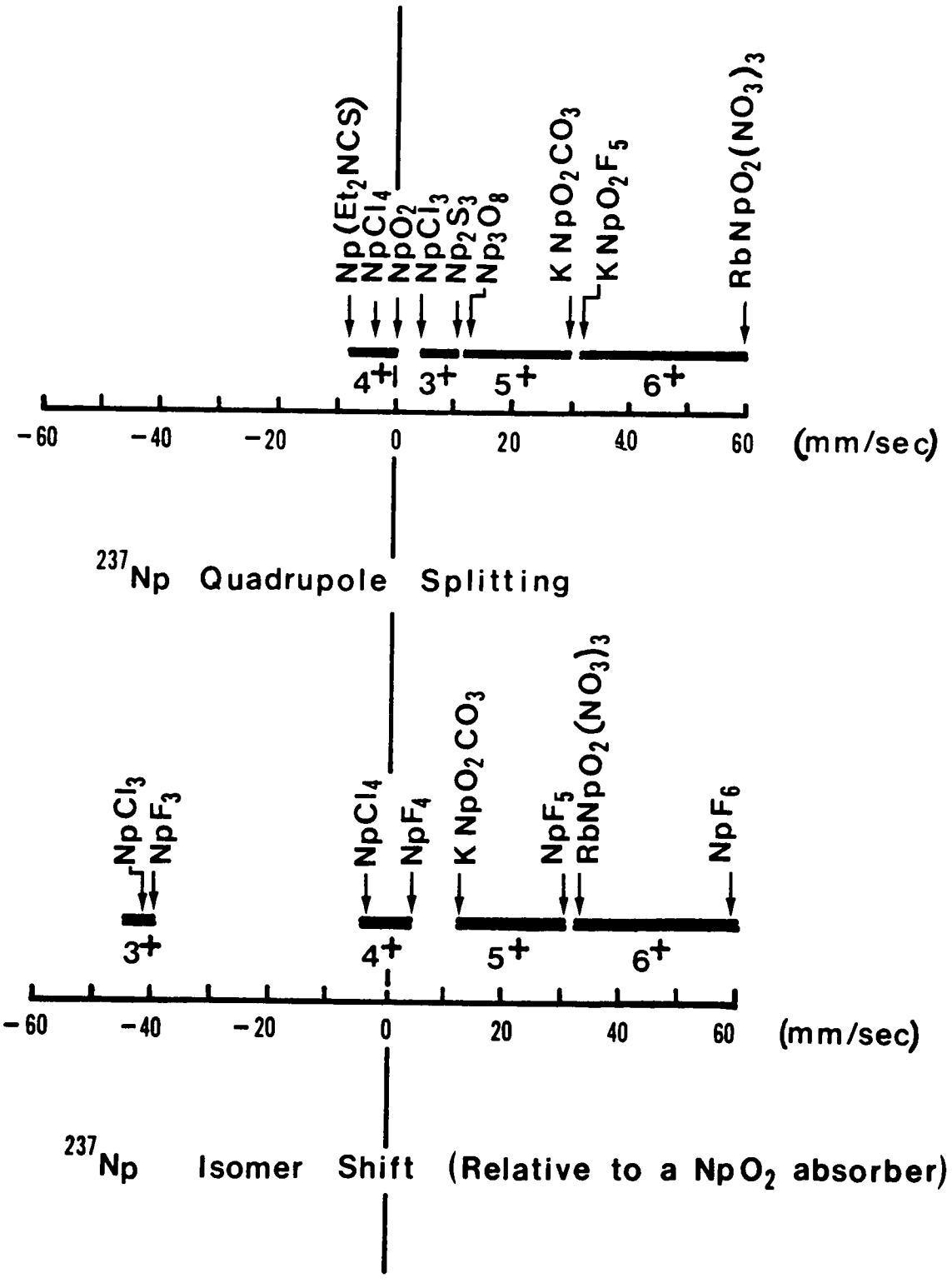

Figure 8. Isomer shifts and quadrupole splittings observed in ^{237}Np grouped by chemical charge states. Positive Doppler velocity means the source compound must be moved toward the NpO_2 absorber for resonant absorption.

monazite. As previously mentioned monazite is monoclinic. Natural monazite is a mixed lanthanide-actinide orthophosphate, that is, Ce, La (Np, Th, U)PO_4. One of the crystallographic results reported by the Oak Ridge group gives the lattice constants of synthetic $CePO_4$ single crystals to be: a = 6.777(1) Å, b = 6.993(1) Å, c = 6.445(1) Å, and β = 103.5°.[22] Each cerium atom has eight oxygen atoms at a distance of 2.5 Å away with a ninth oxygen at a distance of 2.78 Å. The phosphate group, PO_4, takes on the shape of a distorted tetrahedron and links the cerium atoms. Optical studies reported by the Oak Ridge group were performed for a number of lanthanum-actinide mixtures.[2] Lanthanum phosphate was chosen as the host matrix since it is optically transparent. The studies revealed uranium (IV), americium (III) and plutonium (IV) with some evidence for neptunium (IV). It is worth noting that the deep brown color of the La(Am)PO_4 crystals can be annealed out by heating them to 500°C. The crystals then progress from clear to amber and then back to the original dark brown in about 24 hours at room temperature.

Another important measurement employed the technique of electron paramagnetic resonance (EPR). Using this method the Oak Ridge group has verified the equivalence of the substitutional site occupied by Gd (III) ions in single crystals of lanthanum phosphate when grown by the flux technique as compared to crystals from the urea precipitate method. This is an important consideration in applying the Mössbauer results from this work which was done with large single crystals from the flux technique to crystals produced by the industrially suitable urea precipitate method.

II. Mössbauer Results For Am Metal vs. NpO_2

The spectrum of Am metal as a source vs. a NpO_2 absorber was measured at 4.2 K. (In all cases but one, the results quoted in this work are for source and absorber at 4.2 K.) They reveal a single resonance line which was fit by a Lorentzian as given by Eq. (34) on p. 33. The resonance has an isomer shift of 7.89 ± .06 mm/sec and a linewidth (FWHM) of 6.01 ± .2 mm/sec.

The experimental parameters for this combination of source and absorber are summarized in Table III. The high count rate, 140,000 cts/sec, and the relatively large recoilless fraction at 4.2 K made it possible to obtain statistically sound data in about 30 minutes. The measured Mössbauer parameters are summarized in Table IV. Two representative spectra are depicted in Figures 9 and 10 showing a low velocity, higher resolution spectrum and a spectrum taken at the standard velocity, respectively.

Friedt et al.[23] have studied this same combination of source and absorber extensively. For the source and absorber at 4.2 K they obtained a linewidth of 4.0 ± .06 mm/sec and an isomer shift of 7.8 ± .1 mm/sec. The substantially broadened linewidth we observe is probably due to a mixture of phases in the Am metal source. The NpO_2 source used in our work was carefully annealed, as previously outlined, and X-ray results confirmed a cubic structure. The Am metal source on the other hand was not X-rayed. Friedt and his co-workers used a carefully prepared source of α-phase (hexagonal) americium metal, with the structure confirmed by X-ray analysis. Their studies of Am-Pt intermetallics exhibit linewidths from 12.3 to 14.0 mm/sec against an

TABLE III

EXPERIMENTAL PARAMETERS

	Maximum Velocity (mm/sec)	Counts/Channel (millions)	Statistical Error (%)	Run Time (hours)	Count Rate (counts/sec)
Am Metal Source vs. NpO_2 Absorber (4.2 K)	± 58.8	.992	.1	.5	143,600
Am Metal Source vs. NpO_2 Absorber (4.2 K)	± 14.75	.955	.1	.5	135,600
Am Metal Source vs. $NpPO_4$ Absorber (4.2 K)	± 58.8	58.0	.013	23	179,850
$AmPO_4$ Source vs. NpO_2 Absorber (4.2 K)	± 58.8	15.5	.025	43	28,000
$AmPO_4$ Source vs. NpO_2 Absorber (4.2 K)	± 98.0	10.3	.031	30	25,400
$AmPO_4$ Source vs. NpO_2 Absorber (4.2 K)[a,b]	± 58.2	∿ 15.3	.026	∿ 60	18,800
$AmPO_4$ Source vs. NpO_2 Absorber (77 K)[a,b]	± 58.2	∿ 13.2	.028	∿ 48	20,000
$AmPO_4$ Precipitate Source vs. NpO_2 Absorber (4.2 K)[a,c]	± 60.0	∿ 15.0	.026	∿ 23	46,000

[a]Older spectra taken with the NpO_2 absorber before it was heat treated in the reducing atmosphere. Older spectra taken with 1024 channels on the MCA, counts/chennel has been converted to compare with 256 channel data.

[b]Older spectra taken with large single crystals of $AmPO_4$ before crushing to minimize self-absorption.

[c]First run made with $AmPO_4$ precipitated from solution.

TABLE IV

MEASURED MÖSSBAUER PARAMETERS

Experiment	Intensity (% effect)	Relative Intensity (%)	Γ_{exp} FWHM (mm/sec)[a]	1/4 eq Q (mm/sec)[a]	δ_{IS} (mm/sec)[a,b]
Am Metal Source vs. NpO_2 Absorber (4.2 K)[c]	2.36 ± .03	--	5.97 ± .13	--	7.87 ± .03
Am Metal Source vs. $NpPO_4$ Absorber (4.2 K)	.03 ± .01	--	2.77 ± 1.03	--	-3.26 ± .42
$AmPO_4$ Source vs. NpO_2 Absorber (4.2 K)[d]	1.13 ± .06	--	--	--	-6.25 ± .68
Line 1		48.1 ± 2.5	9.04 ± .70	16.5	19.78 ± .27
Line 2		16.4 ± 2.6	5.71 ± 1.93	4.0	-29.06 ± .53
Line 3		26.0 ± 1.9	6.39 ± 1.04	4.0	-41.12 ± .32
Line 4		9.5 ± 1.9	42.7	0.0	-2.8
$AmPO_4$ Source vs. NpO_2 Absorber (4.2 K)[e]	1.20 ± .04	--	--	--	-2.65 ± .57
Line 1		51.8 ± 1.7	9.38 ± .72	16.5	22.92 ± .28
Line 2		17.7 ± 1.4	4.50	4.0	-27.71 ± .44
Line 3		22.9 ± 1.6	7.13 ± 1.05	4.0	-41.07 ± .23
Line 4		7.5 ± 1.4	42.7	0.0	-2.8

TABLE IV (continued)

Experiment	Intensity (% effect)	Relative Intensity (%)	Γ_{exp} FWHM (mm/sec)	1/4 eq Q (mm/sec)[a]	δ_{IS} (mm/sec)[b]
$AmPO_4$ Source vs. NpO_2 Absorber (77 K)[e]	.22 ± .02	--	--	--	-21.90 ± .78
Line 1	--	31.6 ± 1.8	9.87 ± 2.50	--	20.54 ± .78
Line 2	--	68.4 ± 3.8	2.00	--	-41.50
$AmPO_4$ Precipitate Source vs. NpO_2 Absorber (4.2 K)[f]	.11 ± .01	--	--	--	-25.82 ± .78
Line 1	--	76.0 ± 3.0	12.21 ± 1.25	4.0	-38.71 ± .33
Line 2	--	24.0 ± 1.3	57.30 ± 14.00	--	15.00

[a] In fitting the spectrum insufficient resolution was available to get a fit for certain parameters. In these cases (designated by the absence of an error associated with the parameter) a value was assigned.

[b] Isomer shifts reported here reflect the source experiment convention. (Positive for source approaching the absorber, negative for source receding from the absorber.)

[c] Composite result for high and low velocity experiment.

[d] Result is for ± 58.8 velocity experiment. This and all subsequent multiline spectra give the overall absorption and isomer shift as well as the individual contributions from the component lines in the spectrum.

[e] Older spectra taken with the NpO_2 absorber before it was heat treated in the reducing atmosphere, and with uncrushed $La(Am)PO_4$ crystals.

[f] First run made with $La(Am)PO_4$ precipitated from solution, used old NpO_2 absorber before heat treatment in reducing atmosphere.

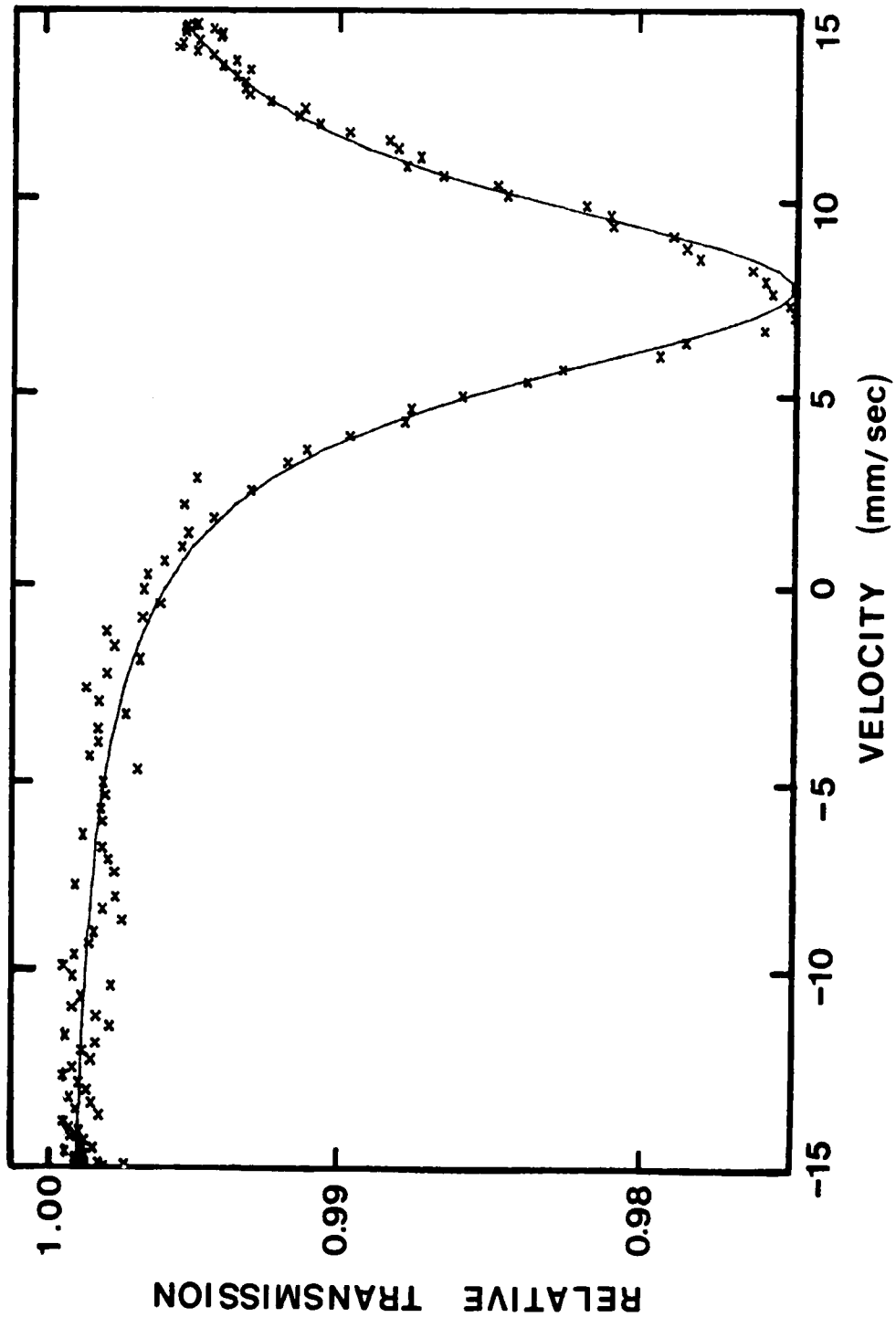

Figure 9. High resolution Mössbauer spectrum of ^{241}Am metal source vs. $^{237}NpO_2$ absorber at 4.2 K. (Positive velocity implies source movement toward the NpO_2 absorber. The statistical error is ± .1%.)

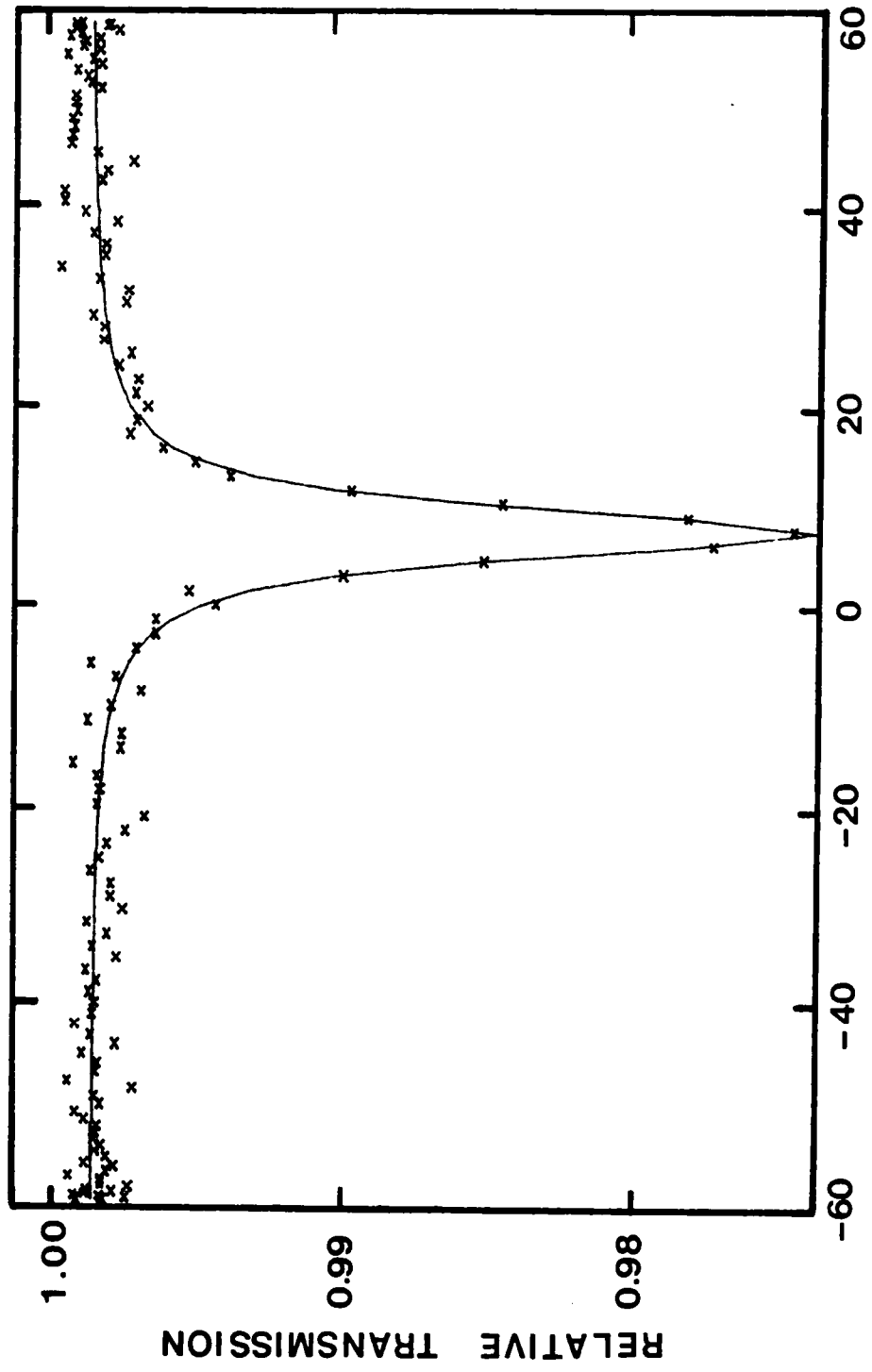

Figure 10. Mössbauer spectrum of ^{241}Am metal source vs. $^{237}NpO_2$ absorber at 4.2 K. (Positive velocity implies source movement toward the NpO_2 absorber. The statistical error is ± .1%.)

NpO_2 absorber (both at 4.2 K). In all cases but one X-ray analysis revealed their intermetallics to have more than one phase. The exception was for $AmPt_5$ which has a hexagonal structure and persists with the broad resonance even though it is a single phase.

The best linewidth obtained by experimenters using the ^{237}Np Mössbauer effect is 1.1 mm/sec which was reported by Dunlap et al.[21] using 5 wt% americium in cubic thorium metal as a source vs. the cubic laves phase compound $NpAl_2$ held at 78 K as an absorber. This linewidth is still roughly 15 times the natural linewidth ($2\Gamma_n$) of .07 mm/sec for the 98 ns mean life, 59.5 keV γ-resonance of ^{237}Np. While $NpAl_2$ gives the best linewidth for a Mössbauer absorber it is also magnetically ordered below 57 K, making it excellent for calibration purposes but unsuitable as an absorber in source studies which require a higher recoilless fraction and thus must be run at 4.2 K.

The single line NpO_2 absorber is the best absorber for source studies but it does have some poorly understood characteristics at low temperature. In the literature some authors[23] state that NpO_2 is weakly ordered magnetically below about 22 K, while others[24] assert that NpO_2 undergoes a transition to antiferromagnetism below 25 K. A survey of the most recent literature shows both properties are still cited. Recent X-ray scattering results show that a phase transition occurs at 25 K and that these lattice changes can mimic a magnetic transition.[25] The important effect observed is a substantial broadening of the γ-resonance in NpO_2 below about 22-25 K. For this reason NpO_2 is often held at about 30 K to get the maximum benefit from the higher Debye-Waller factor at low temperature without the disadvantage of the

broadened line below 22 K. As an example of the linewidth variation. Dunlap and his co-workers[21] found it decreased from 4.1 mm/sec to 3.2 mm/sec when the NpO_2 temperature was raised from 4.2 K to 78 K relative to the Am metal source maintained at 4.2 K. Raising the Am metal temperature to coincide with the 78 K absorber temperature further decreased the linewidth to 2.6 mm/sec. Changes in linewidth for both source and absorber are confirmed in other studies and are attributed to a distribution of the hyperfine interactions changing with temperature. One contributor to this process, about which we will have more to say later, is paramagnetic relaxation.

III. Mössbauer Results for $AmPO_4$ vs. NpO_2

The Mossbauer spectrum for Am in a host matrix of $LaPO_4$ vs. a NpO_2 absorber at 4.2 K has been measured over two velocity ranges and is presented in Figures 11 and 12. An earlier set of spectra is presented in Figures 13 and 14 using an NpO_2 absorber which has not been heat treated and $La(Am)PO_4$ crystals before crushing. This set of spectra shows a comparison of the spectrum at 4.2 K and 77 K. Finally, Figure 15 shows the earliest spectrum taken from an $AmPO_4$ precipitate. (Information was not available on this source, thus it was not discussed in the experimental section.) From the data it is impossible to deduce the precise mechanism causing the various lines in the spectrum. Several possible explanations are presented. One should bear in mind that source studies of Am in various insulating compounds have shown a complex dependence of the measured hyperfine parameters on the temperature, the preparation method and even the elapsed time since source preparation. Thus, the conclusions drawn from this data are relevant only for Am in the $LaPO_4$ host prepared as outlined in the experimental chapter.

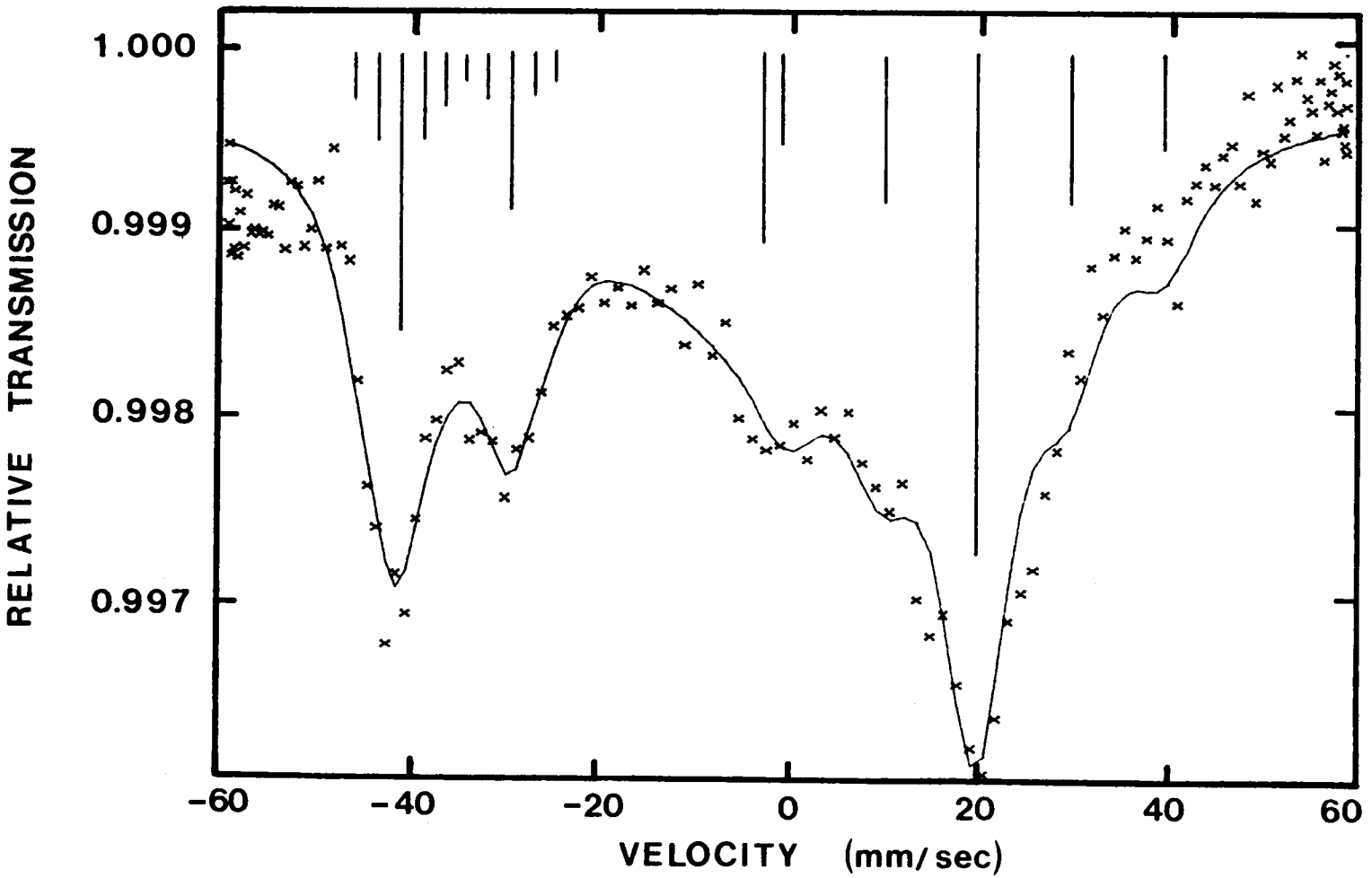

Figure 11. Mössbauer spectrum of $^{241}AmPO_4$ source in $LaPO_4$ vs. $^{237}NpO_2$ absorber at 4.2 K. (Positive velocity implies source movement toward the NpO_2 absorber. The statistical error is ± .025%.)

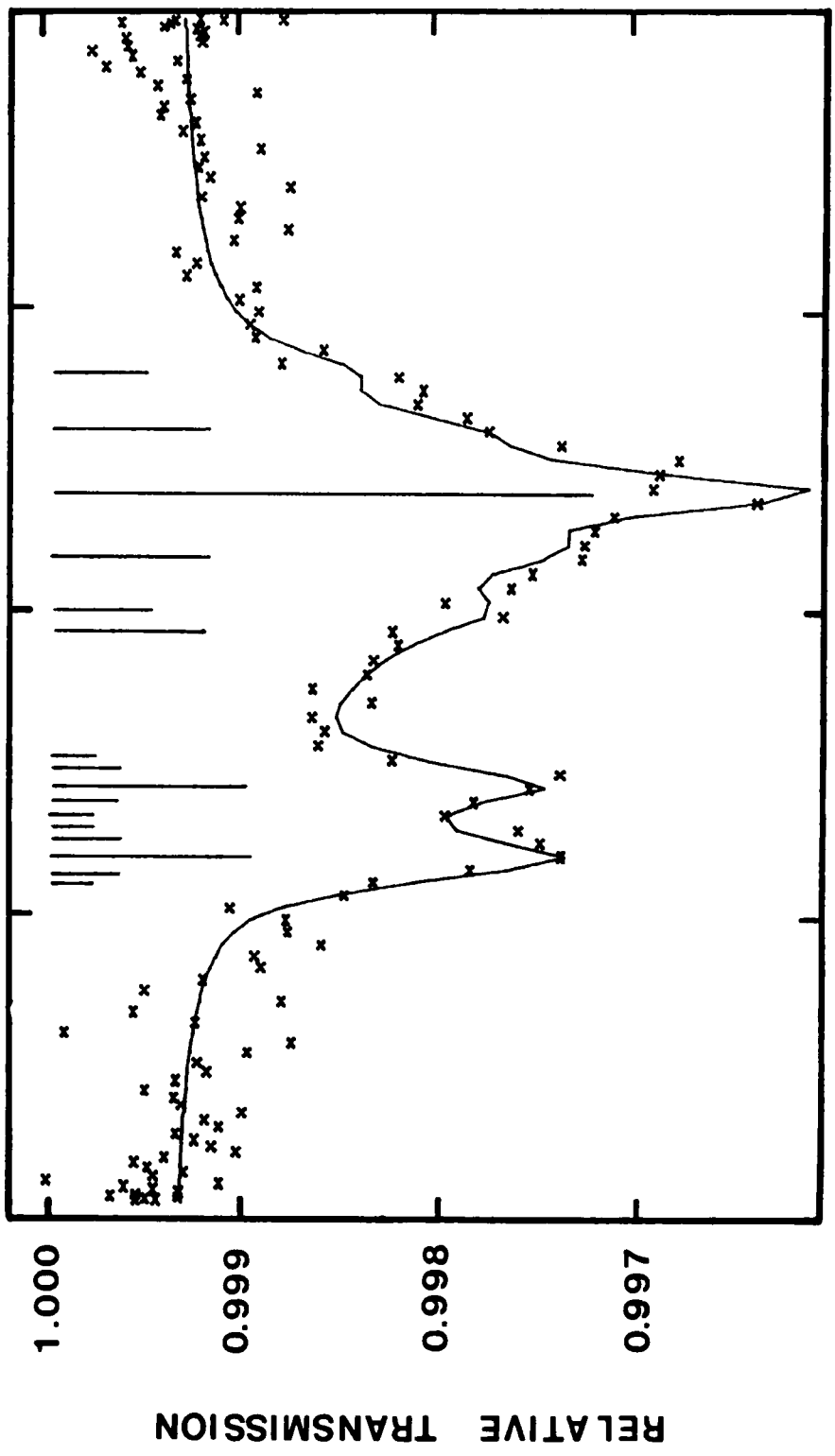

Figure 12. High velocity (low resolution) Mössbauer spectrum of $^{241}AmPO_4$ source in $LaPO_4$ host vs. $^{237}NpO_2$ absorber at 4.2 K. (Positive velocity implies source movement toward the NpO_2 absorber. The statistical error is ± .031%.)

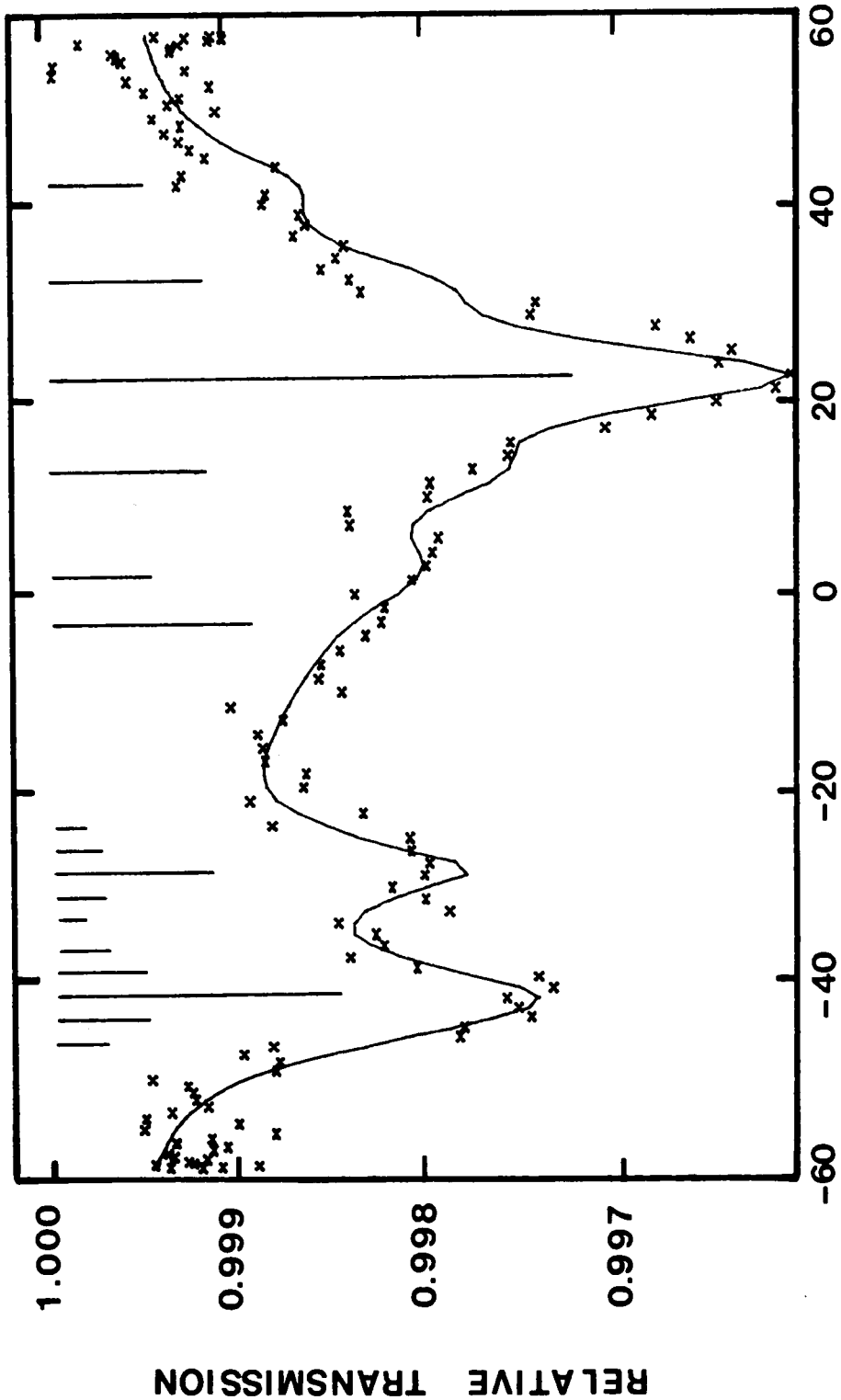

Figure 13. Mössbauer spectrum of $^{241}AmPO_4$ source in $LaPO_4$ host (before crushing crystals) vs. $^{237}NpO_2$ absorber (before heat treating in a reducing atmosphere) at 4.2 K. (Positive velocity implies source movement toward the NpO_2 absorber. The statistical error is ± .026%.)

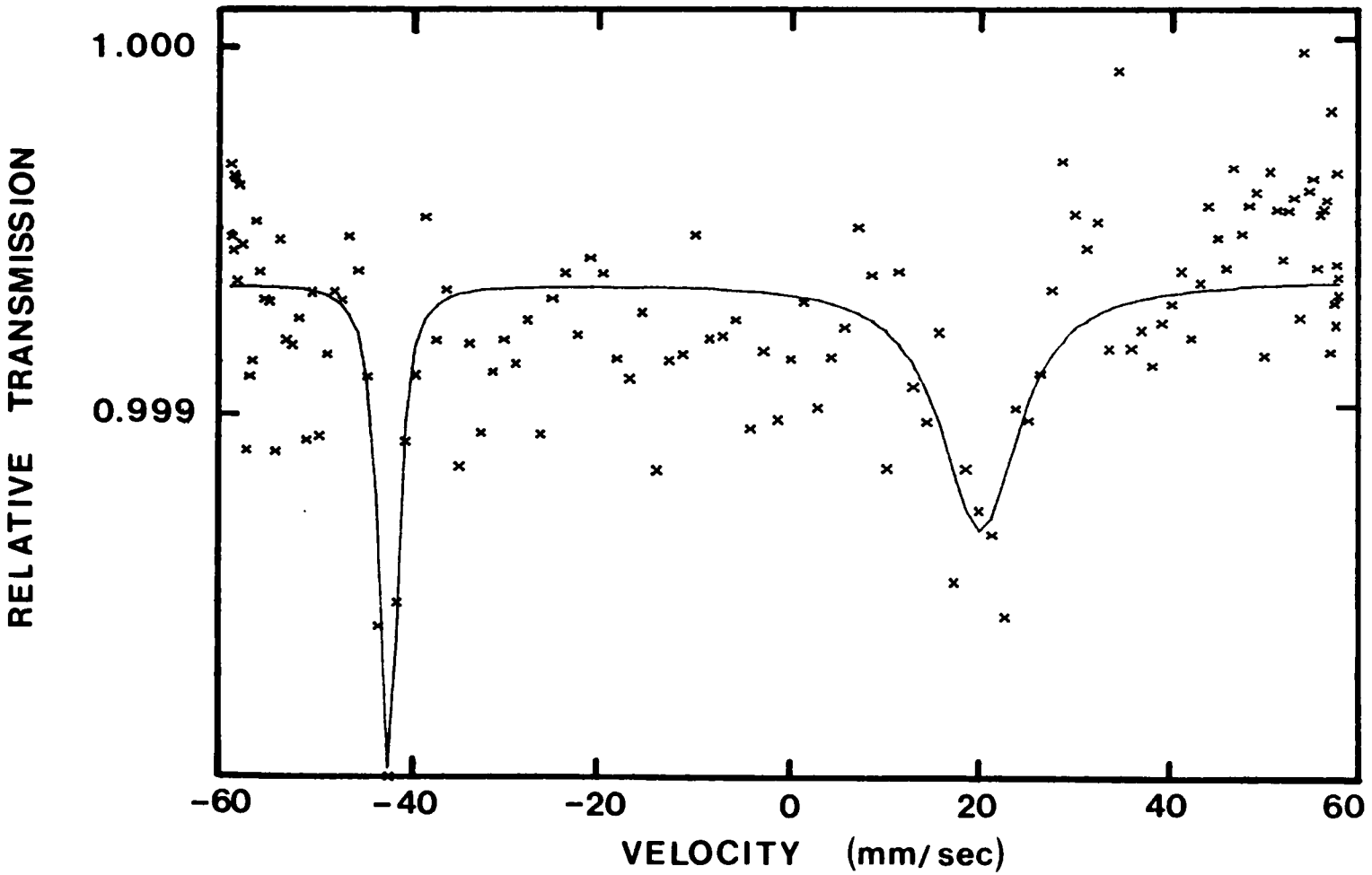

Figure 14. Mössbauer spectrum of $^{241}AmPO_4$ source in $LaPO_4$ host (before crushing crystals) vs. $^{237}NpO_2$ absorber (before heat treating in a reducing atmosphere) at 77 K. (Positive velocity implies source movement toward the NpO_2 absorber. The statistical error is ± .028%.)

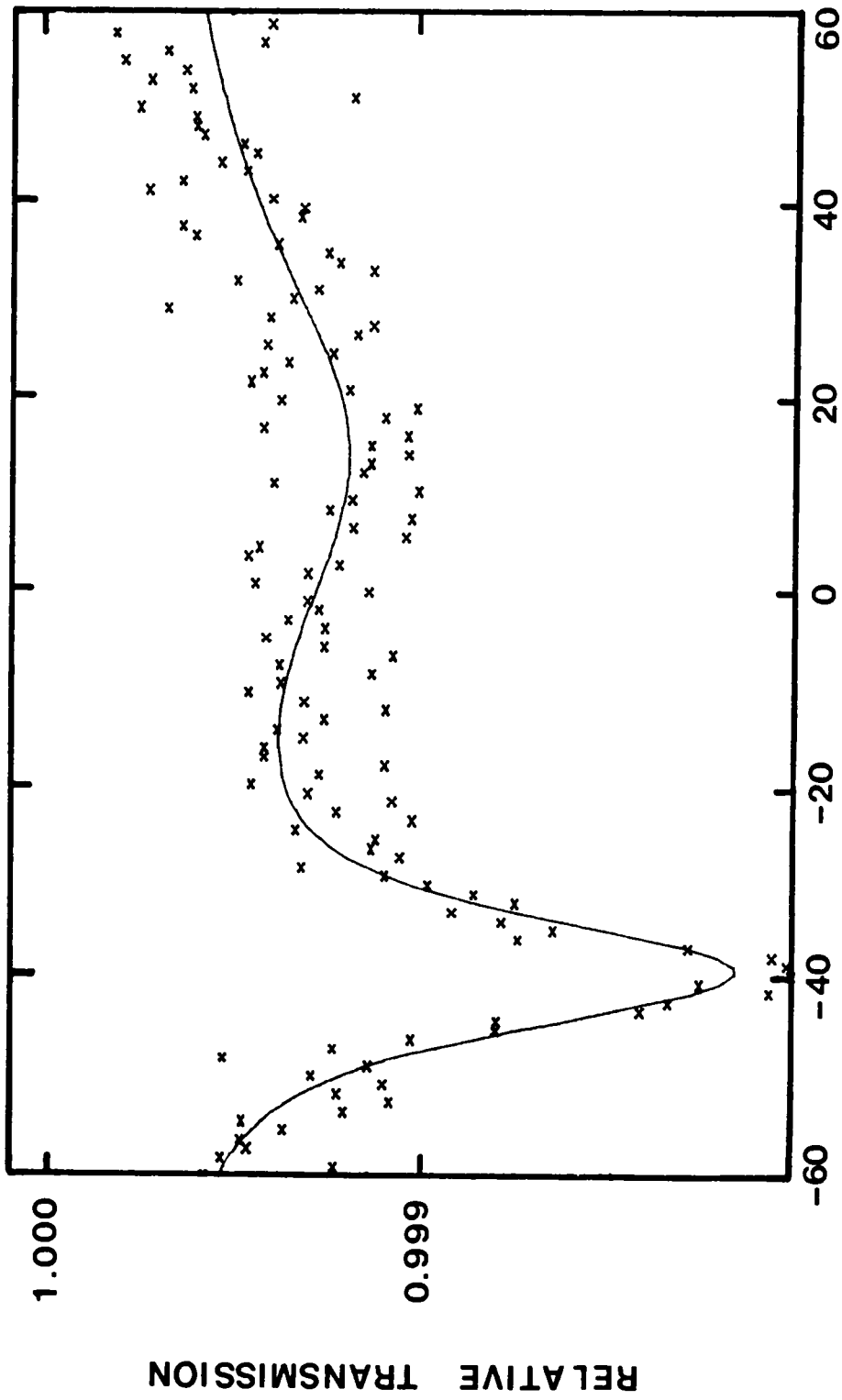

Figure 15. Mössbauer spectrum of $^{241}AmPO_4$ precipitate source vs. NpO_2 absorber (before heat treating in a reducing atmosphere) at 4.2 K. (Positive velocity implies source movement toward the NpO_2 absorber. The statistical error is ± .026%.)

The observed hyperfine interactions are influenced by the local environment of the excited Np atom at an average time of 98 ns after the α-decay of the parent Am atom. Any consideration of the local environment surrounding the excited Np atom in the source must begin with the violent recoil of Np following the α-decay. The α-particle leaves the daughter atom with an energy of 5.5 MeV. According to the Bohr postulate, if the velocity of the α particle is greater than the velocity of the most tightly bound $^4He_2$ orbital electron, then it will leave the atom as a doubly charged ion. According to this postulate an α particle with an energy of more than 400 KeV will leave the atom without electrons.[26] Thus, Np will be left in a reduced state relative to the parent ion. For an Am (III) parent this would correspond nominally to a Np (I) charge state. The energy of the Np recoil is given by $E_{Np} = (m_\alpha/M_{Np})E_\alpha$ which is 93 KeV. This is very large compared with the typical displacement energy in the lattice of ∿ 25 eV, and it indicates that the atom will break loose and move through the lattice losing energy in collisions. Calculations have been done which show that ∿ 1800 defects are produced along a path of 10^{-6} cm and the time required to come to rest is ∿ 4×10^{-13} second in a metallic lattice.[27] This path (∿ 50-200 lattice sites) is generally thought of as a typical displacement for a 93 KeV Np ion.

Charge spectrometry studies which trace the electronic consequences of α-decay by ^{241}Am have been cited by Friedt to argue that the recoiling atom comes to rest with the same valence as the parent atom.[28] This conclusion is based on several assumptions which are: (1) that the Np atom is brought back to the original oxidation state of the parent before recoil (implying a very fast electronic relaxation

time without any Auger processes), (2) that the velocity of the recoiling 93 KeV Np nucleus ($\sim$ c/1000) is less than the velocity of the least tightly bound electron, and (3) that the charge spectrometry results which were done for Am and Np in a gas phase are applicable to a solid. All three assumptions are questionable, the first because the electronic relaxation would depend on the conductivity and temperature of the host, the second since the velocity of the recoiling atom, c/1000, is on the same order of magnitude as the velocity of a 5f electron, and the third since a solid is known to act as a "charge stripper" much more effectively than a gas, removing electrons from the atom as it passes through. The degree to which electron loss occurs is not known but it is believed that in $LaPO_4$ the Np atoms come to rest with a distribution of electron deficiencies which must be compensated for by the surrounding material. Friedt's results with the monoclinic Am_2O_3 source support this picture, although he fails to comment upon it. His spectra indicate the presence of an Np (VI) state at low temperature which vanishes at higher temperatures where electronic relaxation is faster.

To further complicate the picture, the local lattice will have been disturbed by the recoiling Np atom creating a locally elevated temperature which may reduce the recoilless fraction (the "heat-spike" picture). This effect is thought not to be important since comparison with source studies fed by the β^--decay of ^{237}U reveal little difference in the recoilless fraction.[29] There is also the problem of location in the lattice if nonequivalent rest sites are present either naturally or due to radiation damage. The important question from a waste isolation viewpoint is then on what time scale does the relaxation occur or does it occur at all for the various local disturbances.

Time Dependent Hypothesis

The first explanation for the result observed for the excited Np in the $LaPO_4$ is a time dependent one. Assuming that the Np atoms are in a nonequilibrium charge state following the violent recoil one would expect the ions to relax to the equilibrium charge state in some finite time. For a metal this time is on the order of 10^{-12} second, but may be substantially longer in a highly isolating environment.[30]

The multiline spectra of Figures 11 through 14 show the presence of several charge states. Figures 11 and 12 are spectra taken for the $AmPO_4$ source in the $LaPO_4$ host vs. a NpO_2 absorber as described in the experimental chapter. The most intense line is at 19.78 ± .27 mm/sec with a relative intensity of 48.1 ± 2.5% and corresponds to Np (V). There is another intense line at -41.12 ± .32 mm/sec with a relative intensity at 26.0 ± 1.9% which is due to Np (III). The line at -29.06 ± .53 mm/sec with intensity 16.4 ± 2.6% is probably due to a covalent Np (IV). Finally, there is a highly broadened line placed at -2.8 mm/sec to account for the general parabolic bow of the spectrum and is thought to be due to Np (IV). All of the lines are thought to be split by a quadrupole interaction. The Np (V) line is assigned the largest splitting with 1/4 eq Q = 16.5 mm/sec in keeping with the general tendency for Np (V) lines to show a large splitting (see Figure 8, p. 35) while the Np (III) and the covalent Np (IV) are given splittings of 1/4 eq Q = 4.0 mm/sec. No splitting was assigned the Np (IV) line since it was already so broad. Notice that the linewidth observed for Np (V), 9.04 ± .70 mm/sec, is much more than that for the covalent Np (IV), 5.71 ± 1.93 mm/sec, or for Np (III), 6.39 ± 1.04 mm/sec. It is believed that this is possible evidence that the ions are

in the process of relaxing to the (III) charge state of the parent atom. This would be expected if (III) was the equilibrium charge state for Np in $LaPO_4$ and if the Np ions came to rest in the lattice in a more highly oxidized state than the equilibrium charge state. The spectrum of Figure 13 shows the same lines and linewidth relationships except that the lines are generally a little broader indicating that the old NpO_2 absorber before heat treating was probably a broader resonant absorber. The spectrum in Figure 14 which uses the older source and absorber used for the spectrum of Figure 13 shows the usual linewidth narrowing at higher temperature. This experiment at 77 K shows a higher percentage of Np (III), 68.4 ± 3.8%, to Np (V), 31.6 ± 1.8%, adding further evidence to a relaxation picture.

The linewidth observation supports the time dependent argument since the Heisenberg uncertainty principle would predict that those γ-resonances which occur earlier than the 98 ns mean life would also have the broadest resonance. Those earlier resonances would also be the ones which would reflect the most highly oxidized state present and in sufficient quantity to be measurable on the 98 ns time scale. Likewise, those γ-resonances occurring later in time would have the narrowest linewidth and would be expected to reflect a distribution of charge states nearer to the equilibrium value.

This hypothesis is highly speculative especially since the linewidths we are dealing with are already highly broadened from an expected natural linewidth of .07 mm/sec probably due to paramagnetic relaxation. The validity of the foregoing argument would depend on the broadened linewidth being directly proportional to the natural linewidth.

In addition the electronic reaction time would have to be on the order of 10^5 more sluggish than that in the metallic case.

Charge Stabilization Hypothesis

Another explanation for the presence of multiple charge states at the time of the γ-resonance is that the Np atoms come to rest in a variety of lattice sites. Multiline spectra have long been observed from ^{241}Am decay in insulating materials.[13] Studies of AmO_2 by Friedt as a function of temperature have shown that at the time of γ emission, Np is stabilized in both the (IV) and (V) charge states.[23] Americium in AmO_2 is in a (IV) charge state while the Np which is radiation generated is in the (IV) charge state only 34% of the time with the remainder present as Np (V). The relative percentages of Np (IV) to (V) in the source is observed to be independent of temperature in the range from 15 to 360 K. The lack of a quadrupole splitting for the line corresponding to Np (IV) indicates that the Np atom comes to rest in an unperturbed cubic substitutional site displacing an Am atom. The Np (V) line which does show a quadrupole splitting is believed by Friedt and his co-workers to arise from the Np in a defect lattice site. Since the percentages of Np (V) to Np (IV) remains constant over the temperature range one can only assume that any annealing of the Np (V) sites to Np (IV) cubic sites must occur on a time scale much longer than the 98 ns mean life for the γ-resonance. In their paper the authors note that there is no clear evidence for any annealing of the defect site.

The interpretation by Friedt for the AmO_2 result can also be applied to the spectra of Figures 11 through 14 (pp. 45-48). One may assume in this model that the Np atoms in $La(Am)PO_4$ come to rest either

in a variety of lattice sites, as in Friedt's explanation, or with a variety of charge states which are stabilized on the time scale of the 98 ns mean life of the γ-resonance. The variation in the linewidth with charge state may be accounted for in terms of the paramagnetic character of the individual ions. The linewidths follow the same trend observed for Np in the fluoride compounds. The Np (IV) salt, NpF_4, is highly broadened by paramagnetic relaxation with NpF_5, the (V) charge state, less broadened and NpF_3 or the Np (III) charge state the least broadened of the three. This observation is consistent with the paramagnetic correction factors given for Np ions.[30]

It is also worthwhile to compare our spectrum with that reported by Friedt et al.[23] for Am_2O_3 which is monoclinic like $LaPO_4$ and also has an Am (III) parent. Their measurements, like ours, show a Np (III), (IV) and (V) charge state but, unlike AmO_2, with a strong temperature dependence. At low temperatures the Np (IV) line is seen to broaden significantly and the ratio of charge states present tends to the more oxidized states with the Np (VI) line clearly showing up at 4.2 K. Although this does not disprove the possibility of a stabilization of charge states, it does seem to argue in favor of a relaxation to some preferred charge state or perhaps a preferred set of charge states by either electronic or lattice relaxation.

The spectrum of Figure 15 (p. 49) is included for completeness. This spectrum was the first taken when this work began using an $La(Am)PO_4$ precipitate as the source vs. the old NpO_2 absorber before heat treating. The spectrum shows the strongest resonance at Np (III) with a highly broadened line or mixture of lines spanning the isomer shift range corresponding to Np (IV) and Np (V).

IV. Am Metal vs. $NpPO_4$

The Mössbauer spectrum of Am metal vs. Np in $LaPO_4$ is presented in Figure 16. This was the most difficult spectrum to obtain owing to the very small amount of absorber material and strong-self-absorption by the La in the host. The single resonance at -3.26 ± .42 mm/sec was observed in several repeats of this experiment. Still, the statistics of this spectrum are rather poor and any conclusions drawn from it must be considered tentative until better results are available.

In order to compare this spectrum with the $AmPO_4$ source spectrum one must account first for the fact that this is an absorber experiment (reverse velocities) and second that an isomer shift is present between Am metal and NpO_2 (see Appendix). Thus the relative isomer shift of $NpPO_4$ when compared with NpO_2 is +11.13 ± .5 mm/sec. This isomer shift places Np in $LaPO_4$ somewhere between Np (IV) and Np (V) but closer to Np (V). Several questions arise about the possibility of an Np (V) charge state. It is puzzling why the Np (V) charge state for Np in the $LaPO_4$ as an absorber does not coincide with the isomer shift of 19.23 ± .26 mm/sec observed for the Np (V) in the $LaPO_4$ as a source. One answer to that is in the difference between the two materials. Recall that in the Np doped $LaPO_4$ there is a much larger fraction of Np atoms present (about one Np atom for every 64 La atoms) than Am in the Am doped $LaPO_4$ (about one Am atom for every 540 La atoms). Thus, the local conditions could be different in the Np doped $LaPO_4$ than in the Am doped $LaPO_4$. One should also keep in mind that the Np (V) state in the source sites could be recoil generated following the α-decay and thus quite different from a chemically stabilized configuration.

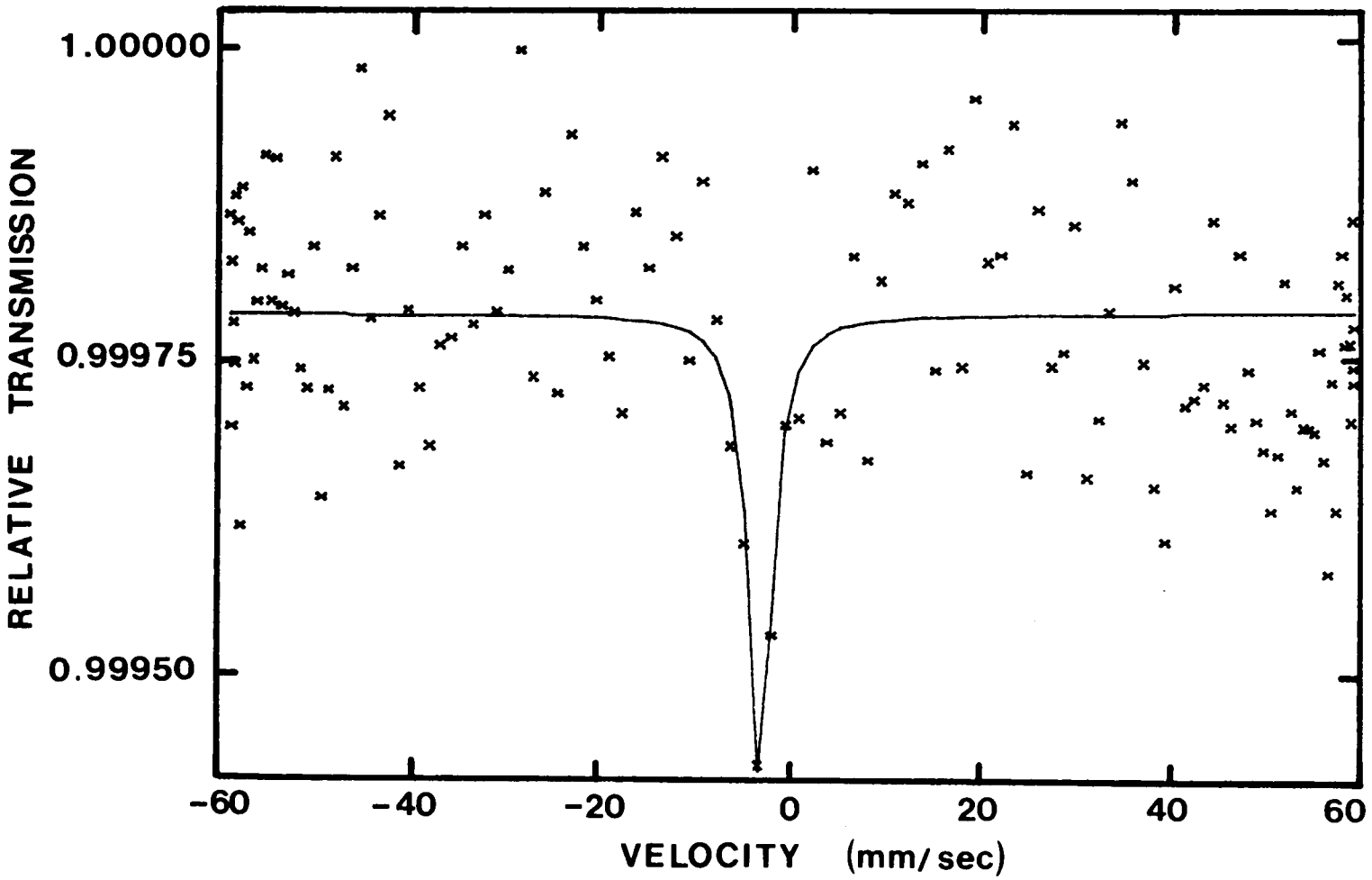

Figure 16. Mössbauer spectrum of ^{241}Am metal source vs. $^{237}NpPO_4$ absorber in $LaPO_4$ host at 4.2 K. (Positive velocity implies Am metal source movement toward the absorber. The statistical error is ± .013%.)

Another problem lies in the narrow linewidth observed in the Np doped $LaPO_4$ absorber. One would expect the paramagnetic broadening at the Np (V) line to be much greater. There is also the absence of any quadrupole splitting to account for. Both of these problems can be blamed on poor statistics. Clearly this spectrum is far from satisfactory but it does offer the possibility that relaxation following α-decay in the Am doped $LaPO_4$ is to the Np (V) charge state and not Np (III) or Np (IV). It should be noted that Np (IV) and Np (V) are both commonly found oxidation states for Np while Np (III) is a less common charge state of Np.

V. Conclusions

The Mössbauer effect has been measured for an Am metal source vs. a NpO_2 absorber, for an Am metal source vs. a Np doped $LaPO_4$ absorber and for an Am doped $LaPO_4$ source vs. a NpO_2 absorber, all at a source and absorber temperature of 4.2 K. The Mössbauer effect has been measured for an Am doped $LaPO_4$ source vs. a NpO_2 absorbed at 77 K. The Am metal vs. NpO_2 showed the standard isomer shift cited in the literature but a broad linewidth. The broadened linewidth was attributed to a mixture of phases present in the Am metal source. The Am doped $LaPO_4$ vs. NpO_2 showed a multiline spectrum with the clear presence of Np (III), Np (IV), and Np (V) charge states at a mean time of 98 ns following the α-decay of the Am parent. The spectrum shows considerable broadening probably due to paramagnetic relaxation. It is not clear whether the three charge states observed are stable or if they are in the process of relaxation to an equilibrium charge state. There is some evidence that relaxation is still occurring at the time of the

γ-resonance. The Am metal vs. Np doped $LaPO_4$ showed a single resonance near the Np (V) charge state with an unusually narrow linewidth. The spectrum is highly questionable due to poor statistics.

Improvement of the results could be obtained by comparing the Am doped $LaPO_4$ vs. NpO_2 result obtained at 4.2 K with a better spectrum taken at 77 K. This would ascertain whether or not relaxation is occurring on a time scale comparable to the 98 ns mean life for the γ-resonance. If a temperature dependence were observed for the relative areas of the Np(III), (IV), and (V) lines, then relaxation would clearly be occurring. It would also be interesting to repeat the experiment at 4.2 K about a year after the result presented here to see if there is any tendency for cumulative radiation damage to induce a change in the charge state distribution. It would be very useful to obtain a better result for the Np doped $LaPO_4$ absorber, preferably with an absorber prepared in the same way as the source. It would also be worthwhile to study the pure crystalline materials $AmPO_4$ and $NpPO_4$ without any lanthanide atoms present. For completeness from a waste isolation standpoint the precipitated $AmPO_4$ and $NpPO_4$ powders should also be studied.

BIBLIOGRAPHY

BIBLIOGRAPHY

1. B. M. Schwarzchild, Physics Today 33, 6, 21 (1980).

2. L. A. Boatner, G. W. Beall, M. M. Abraham, C. B. Finch, P. G. Huray, M. Rappaz, in Scientific Basis for Nuclear Waste Management, Vol. II, edited by C. J. Northrup (Plenum Press, New York, 1980); L. A. Boatner, G. W. Beall, M. M. Abraham, C. B. Finch, R. J. Floran, P. G. Huray, M. Rappaz, Proceedings of the International Symposium on the Management of Alpha-Contaminated Wastes (awaiting publication, Vienna, 1980).

3. The Evaluation and Review of Alternative Waste Forms for Immobilization of High Level Radioactive Wastes, Alternative Waste Form Peer Review Panel, DOE/TIC 10228 (1979).

4. R. L. Mössbauer, Z. Physik 151, 125 (1958); Naturwissenschaften 45, 538 (1958).

5. H. Frauenfelder, The Mössbauer Effect (W. A. Benjamin, New York, 1962).

6. C. M. Lederer, V. S. Shirley, Table of Isotopes (John Wiley and Sons, Inc., 1978), 7th ed.

7. G. M. Kalvius, in Mössbauer Spectroscopy in the Actinides, Proceedings of a Panel (International Atomic Energy Agency, Vienna, 1972).

8. E. A. C. Lucken, Nuclear Quadrupole Coupling Constants (Academic Press, London, 1969).

9. D. G. Karraker, in Organometallics in the F-Elements, edited by T. J. Marks, R. D. Fisher (Reidel Publishing Company, Dordecht, Holland, 1979), p. 395.

10. J. A. Monard, dissertation, Mössbauer Studies of Electrostatic Hyperfine Interactions in ^{238}U, ^{236}U, and ^{234}U, The University of Tennessee, Knoxville, ORNL-TM-3931 (1972).

11. R. L. Mössbauer, Lectures prepared by M. J. Clausen, in Hyperfine Interactions, edited by A. J. Freeman and R. B. Frankel (Academic Press, New York, 1967), p. 497.

12. J. A. Monard, P. G. Huray, J. O. Thomson, Phys. Rev. B 9, 2838 (1974).

13. W. L. Pillinger and J. A. Stone, in Mössbauer Effect Methodology, edited by I. J. Gruverman (Plenum Press, New York, 1968), p. 217.

14. D. O. Patterson, dissertation, Pressure Dependence of the Energy of the Resonance Gamma Ray of ^{197}Au and the Hyperfine Structure Coupling of ^{197}Au in the Ordered Gold-Manganese Alloys, The University of Tennessee, Knoxville, 1966 (unpublished).

15. J. A. Stone, W. L. Pillinger, Bull. Am. Phys. Soc. 11, 309 (1966).

16. Recommendations of the International Commission on Radiological Protection, ICRP (Pergamon Press, New York (1959).

17. R. S. Fiegelson, J. Am. Ceramic Society 47, 257 (1964).

18. Private communication, C. B. Finch.

19. W. S. Aaron, T. C. Quinby, E. H. Kobisk, DOE Report ORNL/TM-6404 (1978).

20. T. J. Kirthlink, Jr., thesis, Effects of Substitutional S-P Metal Impurities on the Mössbauer Isomer Shift of Gold, The University of Tennessee, Knoxville, 1971 (unpublished).

21. B. D. Dunlap, G. M. Kalvius, S. L. Ruby, M. B. Brodsky, D. Cohen, Phys. Rev. 171, 316 (1968).

22. G. W. Beall, L. A. Boatner, D. F. Mullica, W. O. Milligan, J. Inorg. Nucl. Chem. 43, 101 (1981).

23. J. M. Friedt, R. Poinsot, J. Rebizant, W. Müller, J. Phys. Chem. Solids 40, 279 (1979).

24. D. G. Karraker, J. A. Stone, J. Chem. Phys. 70, 2041 (1979).

25. G. Solt, P. Erdös, Crystalline Electric Field and Structural Effects in F-Electron Systems, edited by J. E. Crow, R. P. Guertin, T. W. Máhalisin (Plenum Press, 1980).

26. T. A. Carlson, in Chemical Effects of Nuclear Transformations in Inorganic Systems, edited by G. Harbottle, A. G. Maddock (North Holland Publishing Co., 1979).

27. M. J. Kaplan, J. Inorg. Nucl. Chem. 28, 331 (1966).

28. W. DeWieclawik, Compt. Rend. Acad. Sci. Paris, B266, 577 (1968); W. DeWieclawik, N. Perrin, J. Phys. Paris 30, 877 (1969).

29. J. A. Stone, W. L. Pillinger, Phys. Rev. Lett. 13, 200 (1964).

30. R. Kalish, U. Shreter, J. Grunzweig-Genossar, Hyperfine Interactions, Vol. 1 (1975), 65-80.

APPENDIX

APPENDIX

CONVENTIONS USED IN REPORTING ^{237}Np MÖSSBAUER EFFECT RESULTS

In the course of this experiment difficulty arose in comparing our results with other experiments due to various conventions in reporting Mössbauer isomer shifts. Experiments may be identified as source experiments or absorber experiments, and in comparing the two, one must reverse the sign of one relative to the other. In the source experiment the velocities reported are the actual physical velocities of the source toward the absorber (positive for the source approaching the absorber, and negative for the source receding from the absorber). In the absorber experiment the velocities reported are opposite to the physical velocities. In addition any source or absorber may be compared to another source or absorber even though the experiment has never been done or may not even be possible. These practices make it easy to confuse the assignment of the correct relative isomer shift.

The isomer shift observed in source experiments is the physical isomer shift, or the experimental isomer shift. This may be predicted from Eq. (27):

$$\delta_{IS} = \frac{4\pi}{5} Ze^2 \frac{\Delta R}{R} R^2(|\psi_a(0)|^2 - |\psi_s(0)|^2) .$$

Recall that ΔR is $R_{ex} - R_{gr}$, where R_{ex} and R_{gr} are the "equivalent" nuclear radii for the excited and ground states. For ^{237}Np the value of $\Delta\langle r_N^2\rangle$ is -27×10^{-3} Fm^2. Recall that $R^2 = \frac{5}{3}\langle r_N^2\rangle$ is the equivalent

radius and $\Delta R^2 = 2R^2 \Delta R/R$. If we take $\langle r_N^2 \rangle = (1.2\ A^{1/3}\ Fm)^2$, then $\Delta R/R = 1/2\ \Delta\langle r_N^2 \rangle / \langle r_N^2 \rangle = -2.434 \times 10^{-4}$. There is not complete agreement about this nuclear factor in the literature. However, it is firmly established that this factor is negative indicating a larger equivalent radius for the ground state than for the excited state. Equation (27) then predicts that a positive isomer shift occurs when $(|\psi_a(0)|^2 - |\psi_s(0)|^2)$ is negative, and likewise a negative isomer shift occurs when $(|\psi_a(0)|^2 - |\psi_s(0)|^2)$ is positive. This is in fact what is seen in the experiment. The values of $\Delta|\psi(0)|^2$ have been computed for ^{237}Np for several of the free ion configurations using a relativistic Hartree-Dirac wavefunction code with Slater-Latter exchange and were presented in Figure 4 on page 20.

The form of Eq. (27) makes it easy to predict the outcome of a Mössbauer experiment for a source and absorber which have previously been run against standard sources and absorbers. Consider Figure 17 in which all isomer shifts have been adjusted to coincide with NpO_2 as the zero for the absorbers. One can use this scale to predict the outcome of any experiment possible with the sources and absorbers listed by finding the two relevant isomer shifts on the scale, IS_s and IS_a, the isomer shift of the source and the isomer shift of the absorber. The experiment will show a measured isomer shift of:

$$IS = IS_s - IS_a \ . \qquad (35)$$

As an example of the use of Figure 17 consider Am metal as a source and NpO_2 as an absorber. One would, according to this method, predict

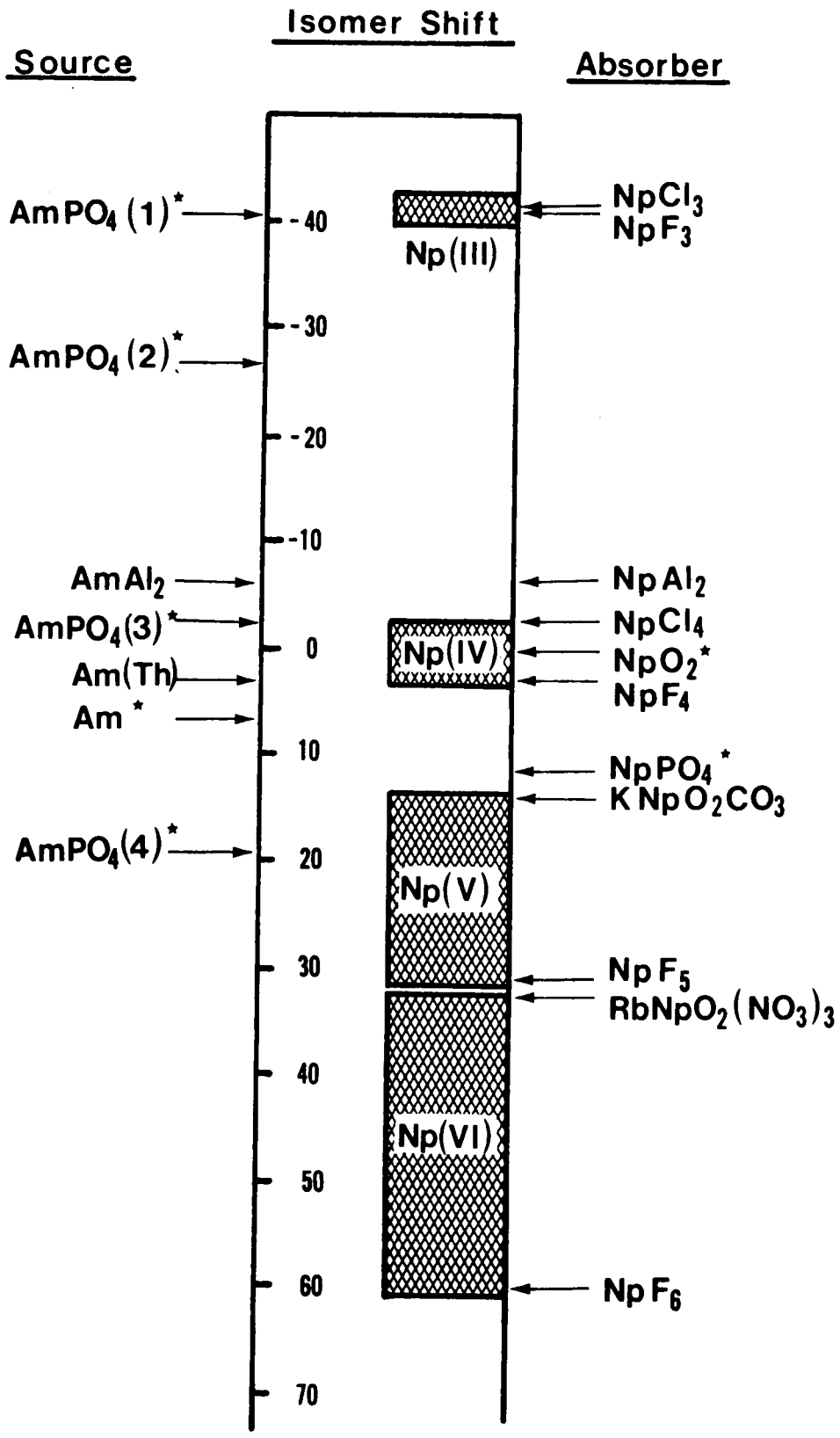

Figure 17. Source and absorber isomer shifts for ^{241}Am and ^{237}Np. Metallic sources are indented. (* indicates measurements made in this work.)

IS = + 7 mm/sec in agreement with Figures 9 and 10 on pages 41 and 42. The sign ambiguity leads to some rather obscure practices in the reporting of isomer shifts in the literature. Friedt et al.[22] report the isomer shift as reversed from the actual Doppler velocity observed in the experiment and justify this by stating that it allows direct comparison with isomer shifts in absorber studies (i.e., source experiments). There is a strong trend to reverse the signs in the results in all the recent studies with the argument that it facilitates direct comparison with older absorber studies.

For this work the following convention has been employed: all experimental results are quoted as source experiments, that is, the actual Doppler velocities observed have been used throughout.

VITA

The author was born November 21, 1954, in Columbia, Missouri. He attended elementary schools in Waco, Texas; Oakland, California; Tainan, Republic of China; and Kennett, Missouri, and graduated from Kennett High School in June of 1973. He entered the University of Missouri, Columbia, Missouri, in June of 1972 and received his Bachelor of Science degree in August of 1976.

After graduation he was employed by Science Applications, Incorporated of La Jolla, California, in the Electromagnetic Division located in Albuquerque, New Mexico. He began study in September of 1978 at the Graduate School of The University of Tennessee, Knoxville, where he received his Master of Science degree in March of 1981.

In September of 1981 he will begin study leading toward the Doctor of Medicine degree at the University of Missouri Medical Center in Columbia, Missouri.

The author is a member of Phi Beta Kappa, Pi Mu Epsilon, Sigma Pi Sigma, and the Society of Physics Students.

He is married to the former Mary Cahill Miller of Hot Springs, Arkansas.